Next generation in-situ sensing on-a-chip (μSoC)

From Concept to Reality: Glucose Responsive Microgel-Based Etalons in Organ-on-Chip Platforms

Master Thesis

C.W.C. van Dongen

Delft University of Technology

TU Delft

Next generation in-situ sensing on-a-chip (μSoC)

From Concept to Reality: Glucose Responsive Microgel-Based Etalons in Organ-on-Chip Platforms

by

Chayenne van Dongen

5184967

Supervisors:	Dr. H. Bazyar
	Dr. B. Fereidoonnezhad
Daily supervisor:	G. Kontaxi
Project Duration:	February, 2023 - December, 2023
Faculty:	Faculty of Biomedical Engineering, Delft

TU Delft

Preface

I extend my appreciation to my supervisors, Dr. H. Bazyar and Dr. B. Fereidoonnezhad, for their invaluable guidance and support throughout the entire process of crafting this thesis. Their expertise and encouragement have been instrumental in shaping the development of my work. And to M. Mastrangeli for accepting the role of external committee member during the defense of this thesis.

A special note of gratitude goes to my daily supervisor, G. Kontaxi, whose consistent assistance and insightful feedback have been integral to the success of this project.

I would also like to express my sincere thanks to Bi/ond (and especially Tawab, Marieke, and Nikolas) for their collaboration, generous assistance, and provision of essential resources. Their involvement has significantly enriched the depth and quality of my research.

Also my appreciation to the University of Alberta and the research group led by Professor Michael Serpe, with special thanks to Nikolas for his invaluable contribution in providing the essential mircogel-beads.

Throughout the course of this research, I have been afforded the opportunity not only to enhance my personal and academic growth but also to showcase my work at MicroTAS 2023 in Katowice, Poland. The privilege of presenting my master thesis at this esteemed conference introduced me to numerous experts in the field of microfluidics. I am deeply appreciative of this enriching experience, as it has significantly contributed to my intellectual and professional development.

Lastly, I want to thank my friends, mom and brother for supporting me along this way and for never getting tired of listening to my stories.

C.W.C. van Dongen
Delft, December 2023

Summary

Organ-on-chips (OoCs) are micro-fabricated cell culture platforms that mimic the function and structure of human organs. Limitations arose in the use of OoCs when they lacked sensing abilities and real-time monitoring. Throughout this thesis, an attempt is being made to address these complications by developing an in situ glucose sensor for OoCs in collaboration with Bi/ond. The foundation of this proof-of-concept is an etalon, consisting of two reflective layers separated by a dielectric layer that allows light to enter and resonate between the reflective layers. The dielectric layer for this purpose will be microgels, with particular emphasis on the biomedical potential of the thermoresponsive polymer poly-(N-isopropylacrylamide) (pNIPAAm). This sensor was developed on silicon and PDMS substrate using evaporation of Cr/Au, spin-coating pNIPAAm-co-10%-AAc and pNIPAAm-co-10%, and mid or post process modification with APBA. Plasma treatment was employed to create a monolithic layer, resulting in a successfully completed fabrication process verified through SEM. Reflectance spectroscopy confirmed the functionality and response, along with an effective generation of a calibration curve for glucose for both substrates and modification processes. The post process approach emerged as more preferable while exhibiting resilience to sterilization procedures that even improved its response to glucose due to removal of unbound APBA during sterilization. Post process samples were used to detect changes in glucose levels in cell medium that had been in contact with C_2C_{12} mouse myoblast cells over 1-, 3-, and 7-day periods. The results showed that the concentration of glucose declined approximately 16 mg/dL after day 1, 130 mg/dL after day 3 and 227 mg/dL after day 7, in comparison to the control measurement. Additionally, there was optical confirmation of the non-toxic effects of the microgel-beads on cell culturing. The investigation of this proof-of-concept of glucose responsive microgel-based etalons was successful, and the next stage would involve integrating this sensor into a chip of Bi/ond.

Contents

Preface i

Summary ii

Nomenclature iv

1 Introduction 1

2 Methods and Material 5
2.1 Pattern etalon . . . 5
2.2 Etalon fabrication . . . 5
2.3 Reflectance spectroscopy . . . 6
2.3.1 Temperature and pH sensitivity . . . 7
2.3.2 Glucose sensitivity . . . 7
2.4 Sterilization . . . 9
2.5 Cell medium and culturing . . . 9
2.6 Biocompatability test . . . 9

3 Results and Discussion 10
3.1 Pattern etalon . . . 10
3.2 Silicon substrate . . . 10
3.2.1 Attempt to create monolithic film of microgel-beads . . . 10
3.2.2 Temperature and pH sensitivity . . . 11
3.2.3 Adding plasma treatment to fabrication process . . . 14
3.2.4 Glucose sensitivity . . . 15
3.3 PDMS substrate . . . 16
3.3.1 Attempt to create monolithic film of microgel-beads . . . 16
3.3.2 Temperature and pH sensitivity . . . 16
3.3.3 Adding plasma treatment to fabrication process . . . 18
3.3.4 Glucose sensitivity . . . 18
3.4 Sterilization process . . . 19
3.5 Cell medium test . . . 21
3.6 Cell culture and biocompatibility . . . 21

4 Conclusion 23

5 Future prospects 24

References 27

A Pattern etalons 30

B Samples 32

C Samples silicon substrate 35

D Samples PDMS substrate 39

E Sterilization 41

Nomenclature

Abbreviations

Abbreviation	Definition
AAc	acrylic acid
APBA	3-aminophenylboronic acid
Au	Gold
Cr	Chromium
EDC	1-ethyl-3-(3-dimethylaminopropyl)carbodiimide
HF	Hydrogen fluoride
LCST	Lower Critical Solution Temperature
OoCs	Organ-on-Chips
pNIPAAm	poly-(*N*-isopropylacrylamide)
PBS	Phosphate-Buffered Saline
PDMS	Polydimethylsiloxane
SEM	Scanning Electron Microscopy

Symbols

Symbol	Definition	Unit
λ_{max}	Maximum wavelength	[nm]
n	Refractive index	[-]
d	Spacing between reflective layers of etalon	[nm]
θ	Angle of incidence	[°]
m	Number of peak	[-]

1

Introduction

Organ-on-chips (OoCs) are micro-fabricated cell culture platforms that mimic the function and structure of human organs. The purpose of OoCs is to improve the quality of *in vitro* testing, for example in the drug development process, by providing *in vivo*-like conditions for the cultured cells [1, 2]. Additionally, OoCs can be used as research tools in fundamental medical research to understand the mechanisms of disease onset and progression [3]. These devices can help in developing personalized medication and treatment without harm to the patient [3]. The increased interest in OoCs is raised from the potential to reduce animal testing, which is problematic due to ethical concerns and the different pharmacokinetic and toxicological effects of drugs on different organisms [1, 2, 3].

Limitations arose in the use of OoCs when they lacked sensing abilities and real-time monitoring. The evaluation of cell status and response to stimuli has traditionally relied on endpoint analyses, primarily utilizing optical and fluorescence microscopy combined with staining and labeling techniques, leading to termination of the experiment [4]. However, these approaches have inherent limitations, as the labels used in such analyses can exhibit non-specific interactions with both cells and the substances being tested. Consequently, the need for label-free and continuous real-time analysis of cell viability parameters persists as a critical unresolved technical complication in the improvement of the OoC models [1, 2].

Throughout this thesis, an attempt is being made to address these complications by developing an *in situ* glucose sensor for OoCs. This thesis is in partnership with Bi/ond, a biotechnology startup in Delft committed to driving progress in biological innovations through the use of engineered microchips. The aim is to explore a proof-of-concept optical sensor capable of detecting alterations in glucose concentration. Ultimately, this technology could be utilized in Bi/ond's MUSbit™ microfluidic chip [5].

The foundation of this optical sensor is an etalon, also referred to as a Fabry-Pérot interferometer [6]. It is comprised of two reflective layers separated by a dielectric layer (see Fig. 1.1a). The distinct design of this setup enables light to enter the space and resonate between the reflective layers (Fig. 1.1b) [7, 8, 9].

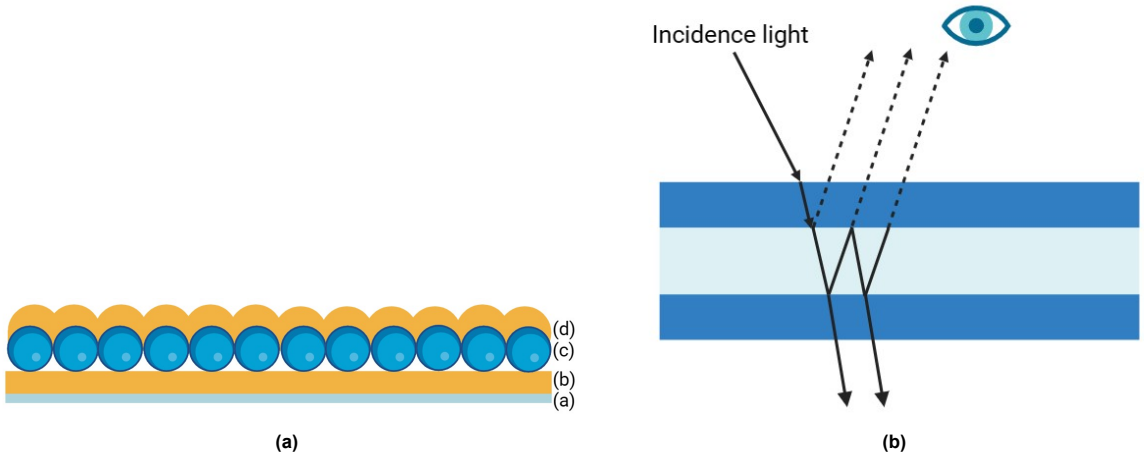

Figure 1.1: Schematic representation of **(a)** etalon structure with (a) substrate, (b) and (d) reflective layers and (c) a dielectric layer and **(b)** Principle of etalon and interference of light inside its cavity (inspired by [10]).

The presence of resonating light generates constructive and destructive interference, enabling the reflection of specific wavelengths of light. These peaks of wavelength positions are dictated by equation 1.1 [8, 9, 6].

$$\lambda_{\text{max}} = \frac{2nd\cos\theta}{m} \tag{1.1}$$

with λ_{max} being the maximum wavelength of the peak, m the peak order, n the refractive index of the dielectric layer, d the spacing between the mirrors, and θ the angle of incidence [8, 6, 9]. From this equation, λ_{max} is directly correlated to d since there is a negligible change in θ and n when inspecting the same peak (m) [9, 6].

The dielectric layer can be made of different materials, based on its application [11]. For this thesis, microgels will be utilized as the dielectric layer. Microgels are hydrogel particles that show colloidal stability and consist of chemically cross-linked three-dimensional polymer networks. In response to diverse external stimuli, including temperature, pH, and enzyme activities, they exhibit significant swelling or shrinking [12]. Especially the thermoresponsive polymer poly(N-isopropylacrylamide) (pNIPAAm) showed great potential for biomedical application [8, 13, 9].

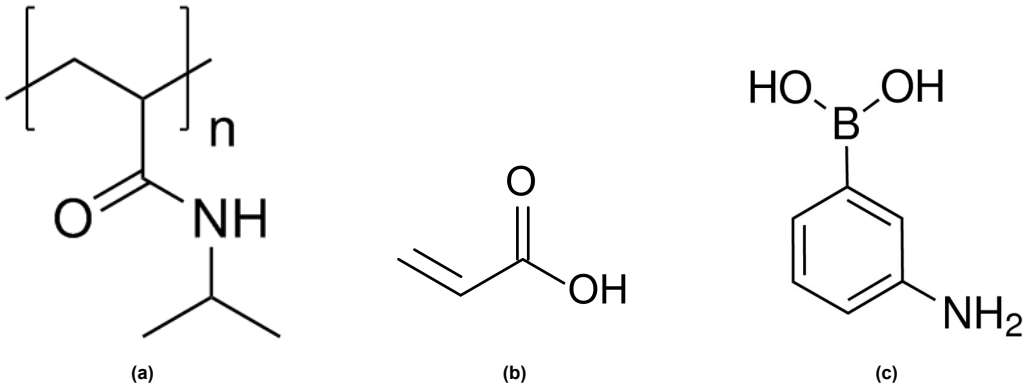

Figure 1.2: Chemical structures of microgel materials used during this thesis: **(a)** poly (N-isopropyl acrylamide), **(b)** acrylic acid, and **(c)** 3-aminophenylboronic acid.

pNIPAAm (Fig.1.2a) is a polymer that displays lower critical solution temperature (LCST) behaviour. When below its LCST (<32°C), pNIPAAm is hydrophilic, swollen, and fully water soluble. Above its

LCST ($>$32°C) it demonstrates a more hydrophobic behaviour and becomes deswollen and water insoluble. This process is fully reversible across multiple iterations. Based on previous researches, the etalon structure consists of pNIPAAm sandwiched between two Cr/Au layers for this thesis [9, 14, 15, 16].
One of the most commonly functional group added to pNIPAAm is acrylic acid (AAc) (Fig. 1.2b) [15]. This monomer is pH responsive and has a pKa of $\sim$4.25. Therefore, at pH$>$4.25, deprotonation of AAc causes a negative charge to the microgel and leads to swelling due to Coulombic repulsion. The microgel is neutral/protonated at pH$<$4.25, leading to a decrease in the swelling. The protonation of AAc causes the microgel to become more hydrophobic [9, 14, 15, 16].

pNIPAAm-co-AAC has been extensively studied and serves as a foundation for the etalons fabricated during this thesis. To create glucose-responsive sensors, pNIPAAm-co-AAC is modified with 3-aminophenylboronic acid (APBA) (Fig. 1.2c). The dissolved phase of APBA-functionalized etalons is dependent on glucose concentration [8, 3]. The pKa of APBA is $\sim$8.2 and submerging the microgel in a basic buffer leads to hydroxylation of the boronic acid component, resulting in negatively charged boron. APBA binds to diols, such a glucose, and they prefere this charged stage. If the pH of the buffer is below the pKa, the binding affinity of APBA to diols is low [17]. The presence of glucose leads to a preference for the bound state to maintain the equilibrium. This promotes additional hydroxylation of boron atoms into a charged form. Due to the same Coulombic repulsion as described earlier for AAc, this leads to swelling of the microgel (Fig. 1.3) [15]. This response is reversible. If the glucose stimulus is removed, there are fewer boronic acid groups in the charged state and thus less strong Coulombic repulsion, resulting in deswelling of the microgel-beads [6].

The swelling increases the distance between the 2 Au layers (d in Eq. 1.1) and results in a wavelength change. The peak's wavelength undergoes a shift within the visible region of the spectrum, transitioning from a red to a blue color (Fig. 1.4). The observed effect is reversible upon the removal of the glucose stimulus [8].

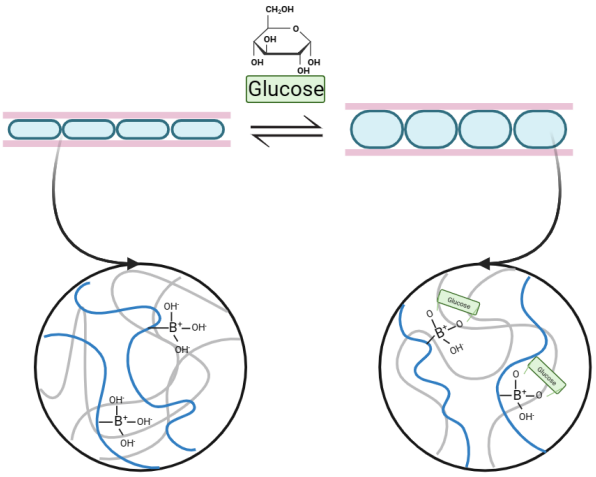

Figure 1.3: Schematic representation of response of APBA-functionalized microgel to glucose in pH=9 (inspired by [8]).

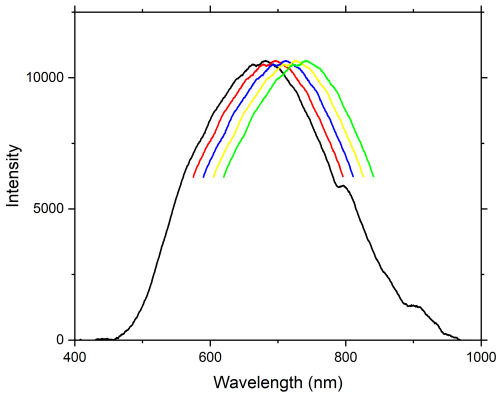

Figure 1.4: Glucose responsiveness demonstrated as a shift from a red wavelength to a blue, yellow or green one within the reflectance spectrum. This depends on the change in distance d between the 2 Au layers. Constructed using pNIPAAm-based microgels modified with APBA (inspired by [8]).

These wavelength changes can be measured using reflectance spectroscopy. This is a rapid, noninvasive monitoring technique that requires no toxic chemicals [18]. It can measure absorption, reflectance, and other properties of solids. The reflection or scattering of light by a solid or particulate medium varies with the wavelength. These changes are due to absorption that depends on the wavelength, and they not only create different colors but also provide information about the material's composition, refractive index, and molecular structure. The distribution of scattered light is influenced by factors like particle size and arrangement within the material [19]. This makes reflectance spectroscopy especially suitable for etalon characterization and validation.

The sensors will be utilized on silicon and polydimethylsiloxane substrates. Silicon is chosen for its fundamental role in microchip fabrication, while PDMS is selected due to its biocompatibility and low toxicity, which aligns with Bi/ond's substrate choice [20].

If a glucose sensor is developed successfully, it undergoes testing with cell medium that has been in contact with muscle cells to determine its ability to measure the glucose concentration in this medium. The final step in confirming this proof-of-concept involves conducting a biocompatibility test by culturing cells on top of the sensor. Biocompatibility assessment is essential for medical devices to verify the capability of a material to function effectively in a particular use case [21]. There are four elements that influence the so called biocompatibility: toxicity, reactions to external organism products, mechanical effects (e.g., stress, compression), and diverse biological interactions with the environment like cell biomaterial interactions [22]. At this stage, the emphasis will be on examining the toxic effects. Polymers often include removable elements like unreacted monomers, oligomers, stabilizers, and processing additives. Similarly, metals (like Cr and Au) can release ions during processes. Toxicologically speaking, this will assess whether the substances can negatively impact the cell growth [22].

Ultimately, the focus of this thesis is to investigate the proof-of-concept of *in-situ* sensing with glucose responsive microgel-based etalons for organ-on-chip application. The findings were encouraging, demonstrating that the fabricated glucose-responsive microgel-beads effectively detected changes in glucose concentrations within cell medium. Additionally, toxicity tests indicated no adverse effects of the etalon material on cell culture. However, additional biocompatibility tests are required to validate these results. Another follow-up would be to implement this microgel-based etalon in Bi/ond's MUSbit™microfluidic chip [5] and to implement this technique to detect other analytes, e.g. lactate.

2

Methods and Material

2.1. Pattern etalon

The initial attempt to fabricate the first layer of the etalon involved covering a 525 μm n-type silicon wafer with aluminum foil, onto which holes were manually punched. While enclosing a wafer was effective, covering only the exposed fractions with gold did not result in a homogeneous pattern. In order to generate an uniform pattern for the etalon, 0.1 mm thick stainless steel (1.4310) sheets of 20 by 20 mm were manufactured with a hole ranging from 0.5-3 mm in diameter (Fig. 2.1). These sheets formed a mask on top of the substrate in order to deposit the Cr/Au layers. In the same dimensions, a bottom mask was also fabricated to securely hold the sample.

2.2. Etalon fabrication

Etalons were made on a 525 μm n-type silicon wafer (with or without Bi/ond's favored PDMS layer) that was first diced into chips of 10 by 10 mm (Disco DAD321, Disco Hi-Tec Europe GmbH). After dicing, the chips were taped to another wafer with the sheet masks on top. Subsequently, a layer of 10 nm chromium and 150 nm gold was evaporated onto the substrate with a rate of 0.100 and 1.50 Å s^{-1}, respectively (Solution PLC-S7, CHA Industries Inc.). The surface of the substrate was plasma treated with oxygen to enhance the formation of a monolithic layer of microgel-beads (Low Power Oxygen Plasma Barrel System Diener Atto, Diener electronic GmbH + Co. KG). The used settings are shown in Table 2.1.

A monolithic polymer layer was created by spin-coating 5 μL pNIPAAm-co-10%-AAc at a velocity of 3000 rpm and a ramp of 2000 rpm/s (Cee®Apogee™Spin Coater, Cost Effective Equipment) on the plasma treated surface. The chips were placed in an oven or on a hotplate at 30°C overnight. The second layer of 2 nm chromium and 15 nm gold was evaporated onto the polymer layer with a rate of 0.020 and 0.150 Å s^{-1}, respectively (Figure 2.2). The surface of the etalons was analyzed using a scanning electron microscope to assess both the size of the microgel-beads and the formation of a monolithic layer (SEM Hitachi Regulus 8230, ST Instruments).

Figure 2.1: Schematic of stainless steel mask used for pattern etalon. The left mask is placed on top of the sample to create a pattern with a diameter ranging from 0.1-3 mm and the middle mask is the bottom mask used to securely hold the sample.

Table 2.1: Settings of the plasma treatment program.

Pumping down period	
Pumping down pressure	0.20 mbar
Gas supply period	
Duration	0.30 seconds
Process gasses	O2 100%
Process pressure	0.25 bar
Plasma process period	
Duration	1.00 minute
Power	100%
Venting period	
Venting time	1.00 minute

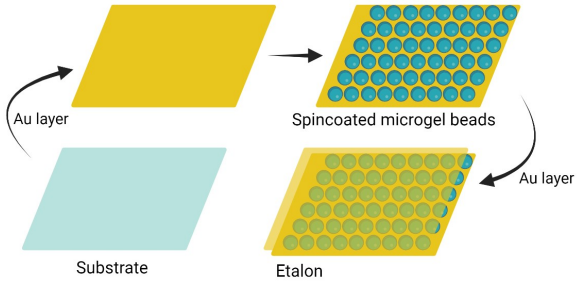

Figure 2.2: Schematic representation of microgel-based etalon fabrication. An underlayer of gold (Au) is deposited on a substrate, followed by a spin-coated layer of microgel-beads. They are enclosed with an overlayer of Au.

2.3. Reflectance spectroscopy

Reflectance spectroscopy is a spectroscopic technique used to validate the fabrication of the etalons by assessing the sensor's responsiveness to various stimuli and examining whether a modification in these stimuli induces a wavelength peak shift. The schematic of the set up is shown in Figure 2.3.

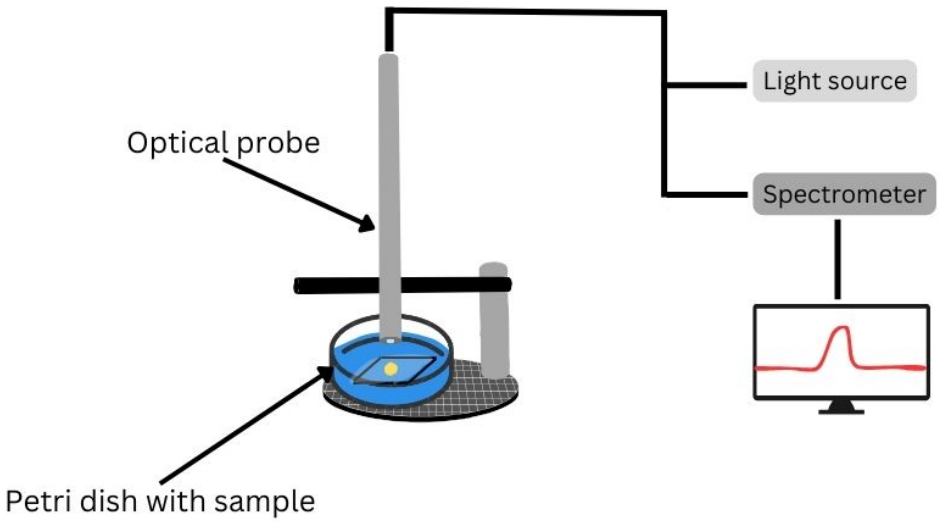

Figure 2.3: Schematic of the reflectance spectroscopy set up (sizes not in proportion).

An optical UV/vis probe (Ocean Insight, Ocean optics CO, LTD) was connected to a light source (Ocean

Insight HL-2000-FHSA, Ocean optics CO, LTD) and a spectrometer (Ocean Insight FLAME Miniature Spectrometer, Ocean optics CO, LTD). The light source was connected to an electrical power outlet, and the spectrometer was linked to a computer via and USB cable. The reflectance probe stand (Thor-Labs, Inc.) was positioned at a height of 55 mm, the tip at 2-3 mm above the sample. Reflectance measurements were conducted using the OceanView 2.0 Ink software with a wavelength range of 400-1000 nm. Only the following parameters were altered from their default settings: Integration time: $\rightarrow$ Automatic, Scans to average: 1 $\rightarrow$ 2, Boxcar width: 0 $\rightarrow$ 25.

2.3.1. Temperature and pH sensitivity

The polymer used to create the monolithic layer, pNIPAAm-co-10%-AAc, is responsive to temperature and pH, respectively. The setup for the temperature experiment deviated slightly from the general configuration displayed in Figure 2.3. In this scenario, the etalon sample was taped to a petri dish and placed on a hot plate set to the desired temperature (Stuart UC152D Stirrer/Hotplate, Cole-Parmer™or SHP-200D-S Stuart Undergrad Digital Stirring Hot Plate, Cole-Parmer™). An additional thermometer was inserted into the petri dish to accurately verify the correspondence between the displayed temperature on the hot plate and the temperature of the liquid within the petri dish (Figure 2.4). Simultaneously, liquid was heated to the same target temperature. Initially, a large droplet was formed between the probe's end and the sample surface to diminish the gap and facilitate wavelength measurement. However, a subsequent approach, involving fully submerging the sample in liquid, proved to yield more reliable results.

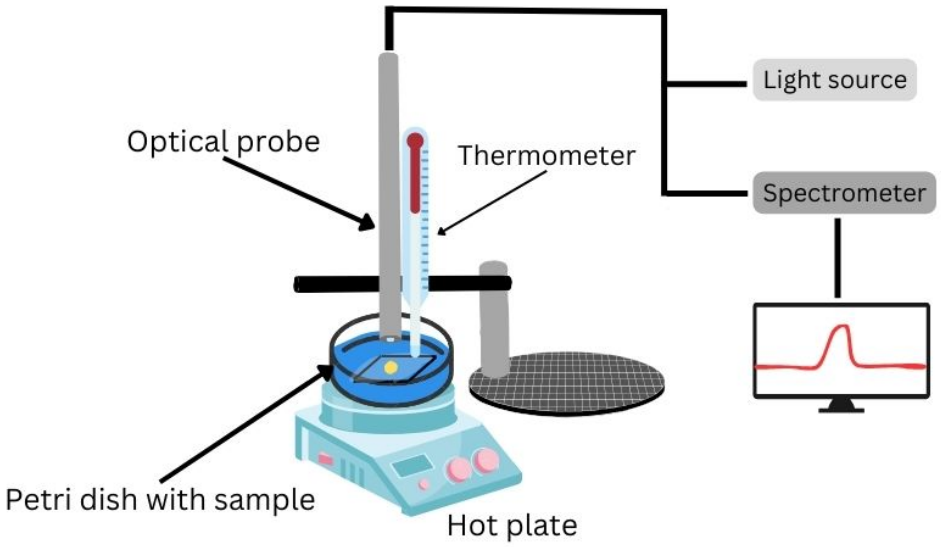

Figure 2.4: Schematic of the reflectance spectroscopy set up for temperature sensitivity experiments (sizes not in proportion).

To validate, the fabricated etalons underwent testing by exposure to 1mM MQ water/NaCl (pH 6.5) at temperatures of 22°C and 35°C, aiming to observe a peak shift in the wavelength. Upon noting this shift, additional tests were conducted involving a broader range of temperature variations (room temperature, 30°C, 40°C, 50°C and 65°C).
To assess the etalons' responsiveness to pH changes, the standard setup was used (Figure 2.3), and the samples were immersed in 1mM HCl/NaCl and 1mM NaOH/NaCl to establish pH environments of 11.0 and 3.0, respectively.

2.3.2. Glucose sensitivity

Microgels responsive to glucose can be synthesized by modifying pNIPAAm-co-10%-AAc with 3-aminophenylboronic acid (APBA). This modification can occur during the synthesis process, resulting in pNIPAAm-co-10%-AAc-APBA, or through chemical modification of APBA after spin-coating pNIPAAm-co-10%-AAc. Both alternatives were explored during this thesis. For the synthesis strategy: pNIPAAm-

co-10%-AAc-APBA was acquired through the supervisor and synthesized following the procedure outlined in [7, 23]. This suspension was spin-coated onto the first layer of Cr/Au instead of pNIPAAm-co-10%-AAc. The same procedure and parameters were used as described earlier in section 2.2.

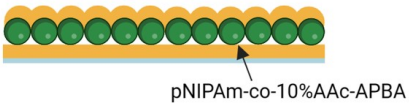

Figure 2.5: Schematic representation of etalon layers with synthesized pNIPAAm-co-10%-AAc-APBA.

Regarding the chemical modification, the procedure outlined in Sorrel (2012) was followed [6]. First, the etalons were placed in BupH™MES Buffered Saline pH 4.7 (instruction on packet were followed, Fisher Scientific™). Next, 9 mg of APBA was added to the buffer and the solution was placed on a stirrer/hot plate for mixing for 1 hour ((Stuart UC152D Stirrer/Hotplate, Cole-Parmer™or SHP-200D-S Stuart Undergrad Digital Stirring Hot Plate, Cole-Parmer™). Then, 20 mg of 1-ethyl-3-(3-dimethylaminopropyl) carbodiimide (EDC) was added to the etalons in buffered APBA solution. After the EDC was mixed to dissolve, the mixture was placed in a refrigerator for 5 hours. Subsequently, 4.5 mg APBA was added per sample to the solution and was placed on the same stirrer/hot plate for 30 minutes. Finally, an additional amount of 20 mg EDC was added per sample and once dissolved, the mixture was put in a refrigerator overnight.

APBA functionalization can be carried out by performing these steps either prior to or following the deposition of the second layer of Cr/Au. They will be referred to as 'mid process' (= before second layer of Cr/Au) or 'post process (= after second layer of Cr/Au).

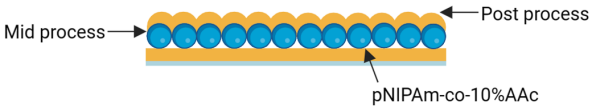

Figure 2.6: Schematic representation of etalon layers with APBA modification before (mid) or after (post) the second Cr/Au layer.

Reflectance spectroscopy was employed to evaluate the responsiveness of the etalons to glucose. The set up shown in Figure 2.4 was used and the etalon was submerged in pre-made concentrations of glucose. A dilution line with set concentrations (0, 20, 40, 50, 60, 80, 100, 150, 200, 250, 300 mg/dL) was used to make a calibration curve by plotting the peak wavelength to the corresponding concentration. This dilution line was prepared by dissolving α-D-Glucose (Sigma-Aldrich®) in pH 9.3 buffer according to the dilution scheme shown in Table 2.2. Between each concentration, there was an approximate 20-minute wait. One etalon was used at least three times to make a calibration curve. This experiment was conducted over 45 times, which includes optimizing the setup, taking measurements on both substrates, and repeating the process on the same sample to generate a calibration curve. An overview of all the samples made during this thesis can be found in Appendix B.

Table 2.2: Measurements to create dilution line with stock glucose concentration of 600 mg/dL

Concentration glucose [mg/dL]	Glucose [mL]	pH 9.3 Buffer [mL]
0	0	15
20	0.5	14.5
40	1	14
60	1.5	13.5
80	2	13
100	2.5	12.5
150	3.75	11.25
200	5	10
300	7.5	7.5

2.4. Sterilization

The sterilization procedure applied to the fabricated glucose-sensitive etalons follows the Bi/ond strategy. The first step was plasma treatment using the same device and settings previously described (Table 2.1). Subsequently, the etalons were immersed for 10 minutes in isopropanol, followed by two additional submerges of 5 minutes each in 10X Phosphate-Buffered Saline (PBS) (Fisher Bioreagents, Fisher Scientific™).

2.5. Cell medium and culturing

An effective way to assess the success of this proof-of-concept for the desired application is by testing the glucose concentration in the cell medium. C_2C_{12} mouse myoblast cells were cultured in Dulbecco's Modified Eagle's Medium D6546 (DMEM, Sigma-Aldrich®) following Bi/onds protocol. To create a calibration curve, different dilutions of this medium were prepared based on the scheme outlined in Table 2.3, with an initial glucose concentration of 450 mg/dL.

Table 2.3: Measurements to create a dilution line using DMEM D6546 medium. The glucose concentration of the medium was 450 mg/dL.

Concentration glucose [mg/dL]	Medium [mL]	Milli-Q [mL]
0	0	10
20	0.44	9.56
40	0.89	9.11
60	1.33	8.67
80	1.78	8.22
100	2.22	7.78
150	3.33	6.67
200	4.44	5.56
300	6.67	3.33
450	10	0

The medium in which the cells were cultured was collected at different time points (one, three, and seven days). The glucose levels in the medium were quantified using the same method described in section 2.3.2. One etalon was used to establish the calibration curve (measured one time), and another to assess the glucose levels in the medium (measured three times).

2.6. Biocompatability test

To evaluate biocompatibility, C_2C_{12} mouse myoblast cells were cultured in a 24-well plate. One well contained a PDMS substrate etalon on a 1 by 1 cm chip, while the other well served as a control without the chip. The chip was coated with fibronectin (50 μg/mL) until completely submerged. Each well was seeded with a cell density of 50,000 cells per mL of medium. After two days, microscopic images were captured and the cells were fixed using PBS washes followed by incubation in 4% paraformaldehyde (PFA) for ten minutes. Subsequently, the chips underwent three PBS washes and were stored at 4 °C in a PBS solution.

3

Results and Discussion

3.1. Pattern etalon

In the first trial to create etalons, a silicon wafer was covered entirely with manually pierced aluminum foil. This approach aimed to gain familiarity with the material's complexities and procedural techniques, as well as investigate the possibility of using a masking technique on a silicon wafer for targeted deposition of Cr/Au in specific areas. This method was later replaced by stainless steel masks to achieve a more uniform pattern (Fig. 2.1). In order to focus on proving the proof-of-concept of these etalons, it was decided to use the largest available pattern size - 3mm - throughout this project. The main objective at this stage is to create a monolithic layer of microgel-beads and measure glucose response; scaling down in size can be considered at a later time. More details about the initial use of aluminium and implementation of the masks can be found in Appendix A.

3.2. Silicon substrate

When attempting to produce etalons on a silicon substrate, various challenges needed to be overcome. This section discusses the main results, while a more comprehensive analysis of all collected data can be found in Appendix C.

3.2.1. Attempt to create monolithic film of microgel-beads

Microgel-beads were functionalized with APBA using various methods to explore the optimal strategy for creating an etalon. The scanning electron microscopy (SEM) images in Figure 3.1 display the microbead results following spin-coating of pNIPAAm-co-10%-AAc-APBA (a), and pNIPAAm-co-10%-AAc with APBA mid (b) and post (c) modification.

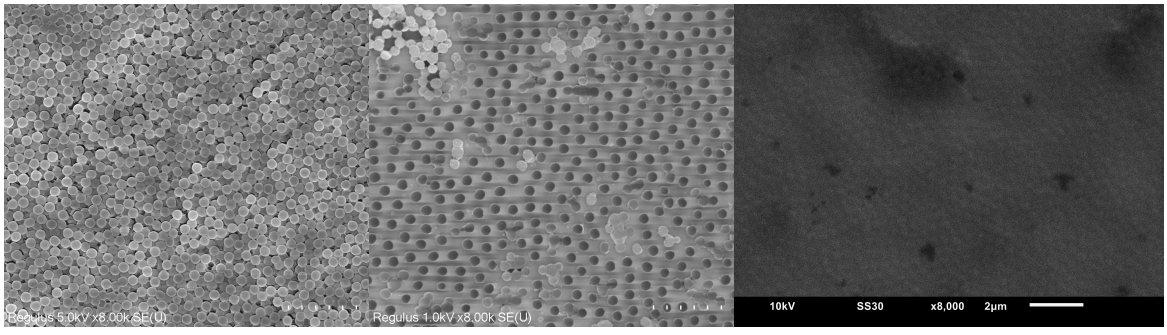

(a) **(b)** **(c)**

Figure 3.1: SEM images of **(a)** synthesized pNIPAAm-co-10%-AAc-APBA, **(b)** APBA modified pNIPAAm-co-10%-AAc mid process and **(c)** APBA modified pNIPAAm-co-10%-AAc post process on silicon substrate.

All methods showed different results. While the synthesized microgel-beads were individual and on top of each other, not forming one layer, the mid process beads showed an individual and dispersed nature, resulting in a striped pattern on the substrate. Agglomeration of the beads was also observed in mid process. An explanation for this behavior may be uncovered by examining the characteristics of the microgel-beads. The spin-coating of both pNIPAAm solutions occurred at room temperature, which is below its LCST of 32°C, and therefore microgels show a more hydrophilic behaviour [6]. Usually, agglomerate formation occurs at temperatures above 32°C, due to the curled formation of the polymer, making it water-insoluble [24, 25].
While hydrophobic attraction was generally presumed to underlie the aggregation process, there exists little to no compelling evidence supporting this hypothesis [24]. Therefore, the dispersion of the polymer could also be caused by another phenomenon called phase separation. Phase separation can induce ordered patterns in thin polymer films. The usual morphology of a film undergoing phase separation is a disordered structure with a specific size. And even though there is some structure, it is not ordered. The interaction between the substrate and polymer is believed to be a key factor contributing to this pattern formation [26].
The same situation applies to these samples. The SEM images reveal distinct patterns in both the synthesized and mid process samples, where the beads were observed to be either stacked on top of each other or spaced out individually. However, the structure of these agglomerates and microgel-beads is not ordered. This may also offer an explanation to the variation in pattern between the synthesized microgel-beads and the modified ones, as they exhibit different configurations of polymers. In contrast, the post process samples exhibited less visible beads during SEM compared to the other two samples, however the beads do seem to be closer together. The reduced visibility of these microgel-beads was caused by the addition of APBA after the second layer of Cr/Au. The conductivity of these samples is lower, since biological material does not conduct [27]. Additional examination of the surface was required to verify whether these beads truly constituted a monolithic layer or if this only appeared to be the case due to the low conductivity.

Reattempts to create a monolithic layer of microgel-beads were made, resulting in more samples with agglomerate formation and spread beads. Especially samples with the synthesized APBA microgel-beads showed no potential in creating a monolithic layer (more data can be found in Appendix A). Therefore the focus turned to optimizing the fabrication process of pNIPAAm-co-10%-AAc mid and post process samples.

3.2.2. Temperature and pH sensitivity

The SEM images provide visual evidence of the successful etalon fabrication, while their functionality is validated using reflectance spectroscopy. The etalons (before plasma treatment) are exposed to different temperatures and pH levels to validate the fabrication process, since pNIPAAm-co-10%-AAc is both responsive to these stimuli.
The etalons were submerged in 1mM MQ water/NaCl (pH 6.5) at different temperatures and the intensity/wavelength graph illustrates how the microgel-beads respond to temperature variations by either swelling or shrinking. This leads to a distance change between the two Cr/Au layers of the etalon, resulting in a shift in wavelength peak. If there are multiple peaks present in the graph, the same one is examined for consistency (m in Equation 1.1).
Etalons prior to chemical modification with APBA and samples following mid process were examined to confirm the manufacturing process and to assess if the modification of the mid process sample with APBA affects the response to temperature and pH. The wavelength at room temperature, 30°C, 40°C, 50°C and 65°C was measured and shown in Figure 3.2. While the results at room temperature are fully detailed, only the peak wavelength is shown for the other temperatures. The peak wavelength corresponding to each temperature is also specified.

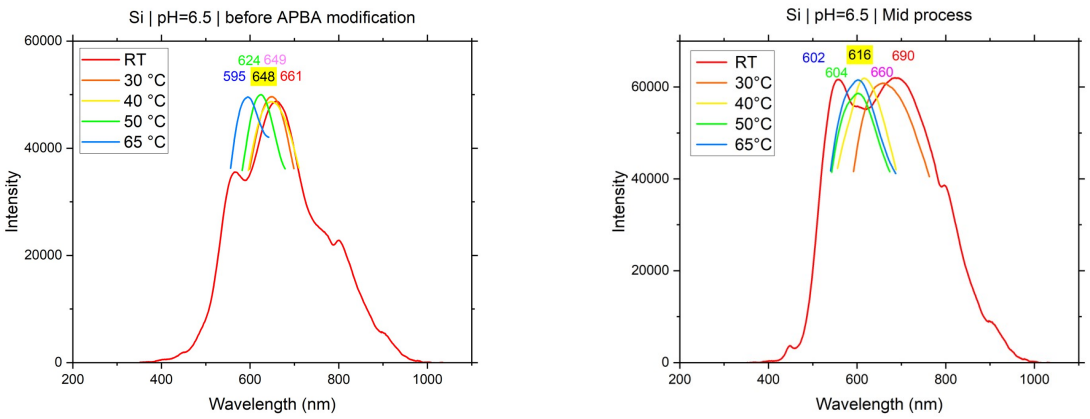

Figure 3.2: Reflectance spectroscopy graphs of temperature measurements on silicon substrate **(a)** before APBA modification and **(b)** mid processed sample. Graph at room temperature is fully displayed, for the other temperatures, only peak wavelength is shown. Corresponding peak wavelength is also specified.

It is apparent that for both samples, as the temperature rises, there was a shift of the peak towards a lower wavelength (blue shift). These results can be explained by the phenomenon that at a temperature below the LCST (<32°C), pNIPAAm is hydrated and fully extended. Intermolecular hydrogen bonding between pNIPAAm chains and water molecules are formed, and the hydrophilic core of the molecule is covered [25, 24]. Above the LCST, intramolecular hydrogen bonds are partially dissociated and thermal energy causes disruption of these bonds [28]. Instead, intra- and intermolecular hydrogen bonds are formed between the carbonyl (C=O) and amine groups (N-H) on the polymer molecules. This configuration causes the molecule to curl up and and shrink, exposing their hydrophobic core, and making them water-insoluble (Figure 3.3) [25, 24]. This also causes the molecules to shrink more if the temperature is increased, leading to further de-swelling of the microgel-beads and hence a reduction in distance d (Eq. 1.1) of the gold layers in the etalon structure and a lower wavelength.

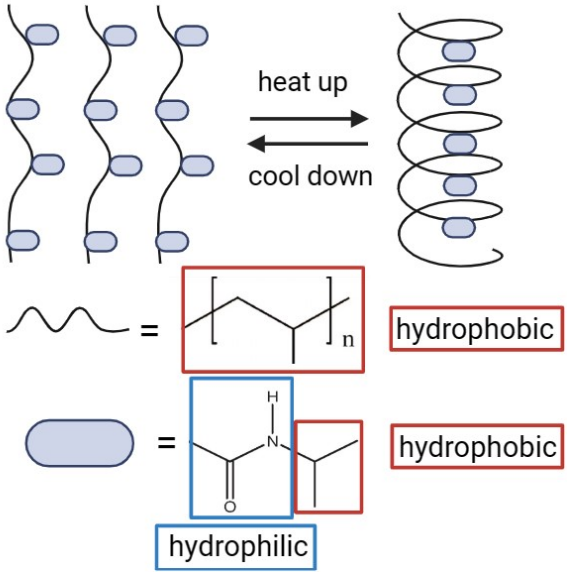

Figure 3.3: Schematic of pNIPAAm behaviour as result of temperature change (inspired by [25]). Red indicate hydrophobic parts of the strucute, and blue a hydrophilic part.

This trend was observed in both samples, regardless of APBA modification, indicating that the inclusion of this step in the production process did not impact the microgel-beads function as anticipated (Figure 3.2).

Even though incorporating APBA into the manufacturing process did not impact the outcomes, there were slight variations in the shapes of the graphs. Although the same peak was monitored (m=3, Eq. 1.1), peak 2 was more pronounced in the pre-APBA modification sample.
Thin film interference may account for the differences in graph appearance. This occurs if there is interference between light reflected from different surfaces of a thin film [29]. This was the situation with microgel-based etalon; two Cr/Au layers that function as reflective layers (as explained in Chapter 1, introduction). To induce the peak shift, it was presumed that the angle of incidence (θ) was negligible, which remains true for the maximum wavelength. However, as the microgel-beads do not create a flat layer but possess a more uneven structure reflecting their shape, the angle of incidence was slightly influenced by this arrangement. Variations in angle of incidence can lead to certain peaks being more pronounced in some samples than others (Figure 3.4) This discrepancy may arise from using slightly different positions for each measurement and from light striking the beads at different angles.

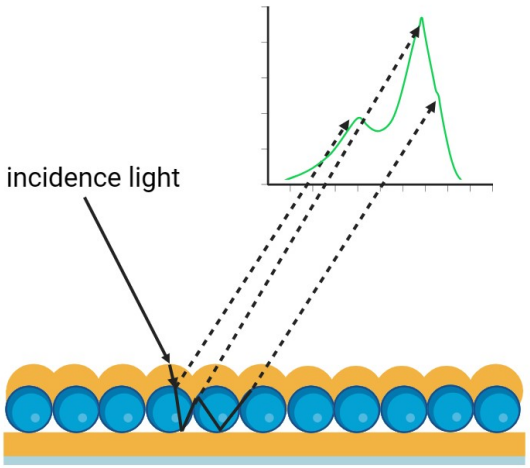

Figure 3.4: Schematic of effect of small changes in angle of incidence (θ) on the reflectance spectra.

The pH sensitivity of the unmodified etalons was tested by submerging them in 1mM HCl/NaCl (pH 3.0), 1mM MQ water/NaCl (pH 6.5) and 1mM NaOH/NaCl (pH 11.0). Reflectance spectroscopy was used similarly to the temperature measurements to validate the fabrication process. The results are shown in Figure 3.5. While the result of pH 6.5 is fully visualized, only the peak wavelength is shown for the other pH levels.

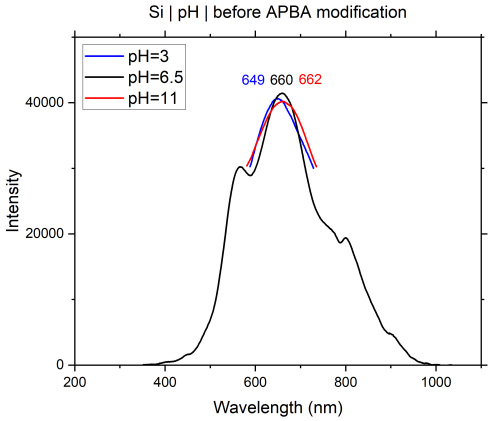

Figure 3.5: Reflectance spectroscopy of an etalon on a silicon substrate submerged in 1mM HCl/NaCl (pH 3.0), 1mM MQ water/NaCl (pH 6.5) and 1mM NaOH/NaCl (pH 11.0) solutions. 1mM MQ water/NaCl (pH 6.5) is fully shown, for the other two pH levels only the peak wavelength is visualized. The maximum wavelength is also presented for each pH level.

The increase in pH level causes an increase in the maximum wavelength (red shift), which aligns with

previous studies ([6, 8]. This is because the AAc group attached to pNIPAAm becomes protonated at a level below the pKa of 4.25, leading to shrinkage of the microgel-beads. Conversely, when the pH level exceeds 4.25, deprotonation of AAc results in a negative charge on the microgel and leads to swelling due to Coulombic repulsion [9, 30, 15]. The observed result from this pH experiment validates the functionality of the fabricated etalons.

3.2.3. Adding plasma treatment to fabrication process

Even though the etalons continued to operate, a consistent layer had not been achieved. As a result, an additional stage was incorporated into the fabrication process in an attempt to produce a monolithic layer. The substrate was plasma treated with oxygen before spin-coating the microgel-beads. Oxygen plasma treatment improved surface wettability and adhesion to a metal surface [31]. The results after plasma treatment are shown in Figure 3.6.

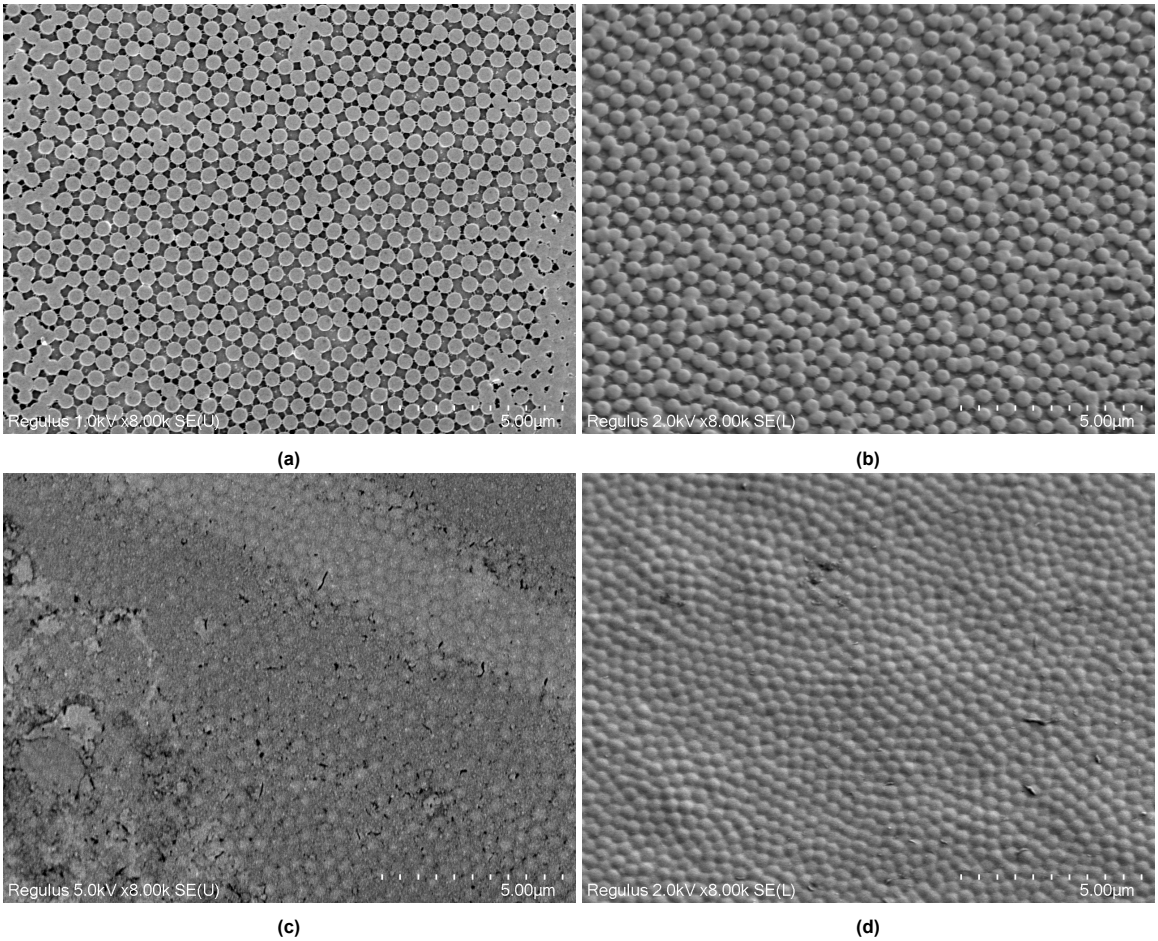

Figure 3.6: SEM images of pNIPAAm-co-10%-AAc mid process **(a)** under 0°angle and **(b)** 30°angle, and post process **(c)** under 0°angle and **(d)** 30°angle. These images were taken after plasma treatment on silicon substrate.

The introduction of plasma treatment during the fabrication process had a notable impact on the dispersion of beads and the formation of a cohesive layer. Both modification techniques resulted in the creation of a single layer of microgel-beads (Fig. 3.6), as opposed to stacked or agglomerated formations (Fig. 3.1). However, there is more spacing between the beads in the mid process samples compared to those treated after processing. This might be due to the presence of APBA surrounding the microgel-beads prior to the evaporation of the second Cr/Au layer, which was not present in the post processed samples. The post processed microgel-beads exhibit closely packed arrangement which represents the desired morphology.

3.2.4. Glucose sensitivity

In addition to the visual confirmation of a monolithic layer of microgel-beads, the crucial aspect was the responsiveness of etalons to glucose, which was also evaluated using reflectance spectroscopy. If a monolithic layer is present but there is no peak shift in wavelength, then the etalon remains non-functional for its intended application. An attempt was made to generate a calibration curve using pre-made glucose concentrations diluted in 5mM Na_2CO_3/$NaHCO_3$ buffer (pH 9.3) at room temperature. These circumstances are anticipated to be the most suitable for the microgel-beads ([6]), which is ideal when constructing a calibration curve. The results displayed in Figure 3.7 illustrate the mean of three glucose measurements on the sample sample. $\Delta\lambda$ was selected over λ_{max} as outcome, as for each set of measurements, the λ_{max} had a different baseline (Appendix C and D.). Analyzing the $\Delta\lambda$ provides a more comprehensive view of the findings.

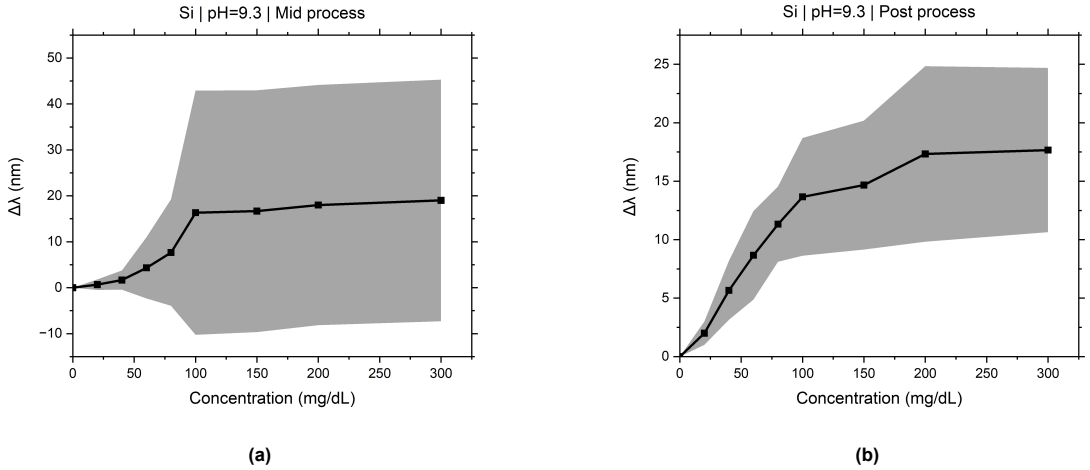

Figure 3.7: Calibration curve of difference in peak wavelength vs. concentration of glucose on silicon substrate on **(a)** mid process sample (average of two measurements) and **(b)** post process samples (average of three measurements). The average of measurements on the same sample are shown as shaded error bars.

The samples were tested three times, however, one series of measurements for the mid process sample was inconsistent and therefore not included in the average values that is shown in Figure 3.7 (for more data see Appendix C, Figure C.6). The calibration plot of the mid process sample appeared distinct from that of the post process sample. At a glucose concentration of 100 mg/dL, it appears that a plateau is formed with the mid process sample, and the error bars indicate a negative change in wavelength. It is improbable for the microgel-beads to contract upon exposure to higher levels of glucose resulting in a decrease in wavelength.

The anticipated trend is more in line with the results observed in the post process sample, where $\Delta\lambda$ increases with glucose concentration. The unexpected results from the mid process samples may be attributed to the microgel-beads not being as densely packed as those in the post process samples (Figure 3.6 (b) and (d)). If these microgel-beads swell and increase their size, they could potentially expand in all dimensions due to surrounding space, leading to expansion in width rather than just height [32]. This scenario would account for the plateau reached in the mid process sample. It is possible that even if these microgel-beads swell by a similar amount as those from later process stages, they might reach their maximum height earlier because of additional expansion into width.

3.3. PDMS substrate

Alongside the silicon substrate etalons, etalons were also fabricated on a polydimethylsiloxane (PDMS) substrate. Due to its affordability, ease of handling, and quick prototyping process for creating small-scale structures, PDMS is one of the most commonly utilized materials in the production of OoCs [33]. Bi/ond also utilized it for their MUSbit™[5]. Therefore, making it an essential material to use. It is also used in other studies as a substrate, because of its Similarly to the silicon substrate etalons, this section focuses on the key results. A more extensive examination of all gathered data can be referenced in the Appendix D.

3.3.1. Attempt to create monolithic film of microgel-beads

Identical approaches for modifying the microgel-beads with APBA were applied to etalons on an PDMS substrate. The SEM images in Figure 3.8 present the deposition of spin-coated (a) pNIPAAm-co-10%-AAc-APBA, (b) pNIPAAm-co-10%-AAc with APBA mid, and (c) post modification.

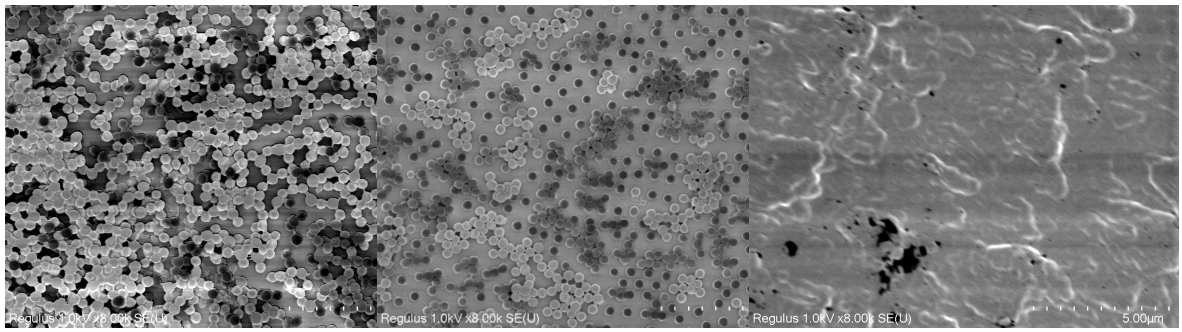

(a) **(b)** **(c)**

Figure 3.8: SEM images of **(a)** synthesized pNIPAAm-co-10%-AAc-APBA and APBA modified pNIPAAm-co-10%-AAc **(b)** mid and **(c)** post process on PDMS substrate.

PDMS is a form of silicon and shares similar properties, such as hydrophobicity [34]. However, the addition of two methylgroups to the siloxane core of the polymer sets PDMS apart from pure silicon [20]. Consequently, the surface materials yield somewhat analogous outcomes. In the case of synthesized beads, they tend to agglomerate and cluster together (Figure 3.8a). Adding APBA before or after evaporation of the second layer of Cr/Au also failed to produce a cohesive film of microgel-beads; instead, the microgel-beads exist either individually or in clusters in mid process samples (Fig. 3.8b). These observations could be attributed to phase separation outlined earlier in section 3.2.1. The morphology displays structured patterns with individual or clustered arrangements but lacks uniform organization on a substrate similar to silicon. As for the post process results, further analysis was required to draw conclusions about this fabrication process, as the microgel-beads exhibit reduced conductivity due to the presence of APBA on top of the second layer of Cr/Au [27].

Multiple samples were produced, and it was observed that pNIPAAm-co-10%-AAc-APBA had less potential to form a unified film of microgel-beads on this PDMS substrate compared to samples modified with APBA. Despite numerous attempts, only clusters formed in the former case, while the modified APBA samples exhibited some form of single-layer coverage although not completely uniform. It was therefore decided that the focus was on optimizing the fabrication process of pNIPAAm-co-10%-AAc mid and post process samples.

3.3.2. Temperature and pH sensitivity

The fabrication process was optically confirmed using SEM images, and functional validation was also pursued using reflectance spectroscopy. The protocol used for the samples on silicon substrate was replicated. Figure 3.9 illustrates the results of temperature measurements on etalons (before plasma

treatment). The full intensity/wavelength graph is presented only at room temperature, while for other temperatures, only the peak wavelength is shown for the mid process samples. The peak wavelength corresponding to each temperature is also specified.

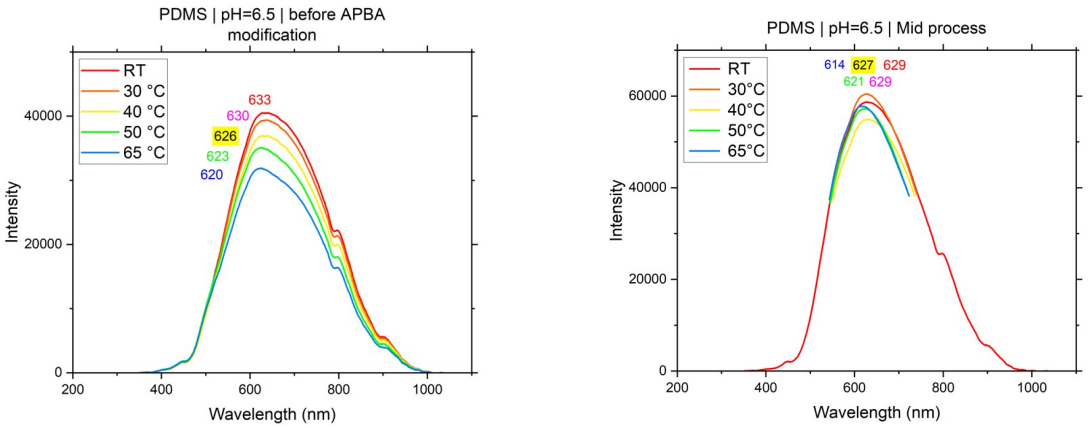

(a) **(b)**

Figure 3.9: Reflectance spectroscopy graphs of temperature measurements on PDMS substrate **(a)** before APBA modification and **(b)** mid processed sample. Graph at room temperature is fully displayed, for the other temperatures, only peak wavelength is shown. Corresponding peak wavelength is also specified.

Similarly, the measurements showed a consistent trend on PDMS substrate as they did on the silicon substrate. As the temperature increased, both the unmodified samples and those in process exhibited a shift in peak towards a lower wavelength. This aligned with expectations, indicating a conformational change in polymer chains leading to deswelling of the microgel-beads [25]. The same peak was monitored and the overall outlook of the graphs with and without APBA modification was more alike in terms of intensity and presence of peaks.

The responsiveness to pH was also validated using the same protocol as described for the silicone substrate samples. The results after submerging the same, unmodified sample in 1mM HCl/NaCl (pH 3.0), 1mM MQ water/NaCl (pH 6.5) and 1mM NaOH/NaCl (pH 11.0) are shown in Figure 3.10. .

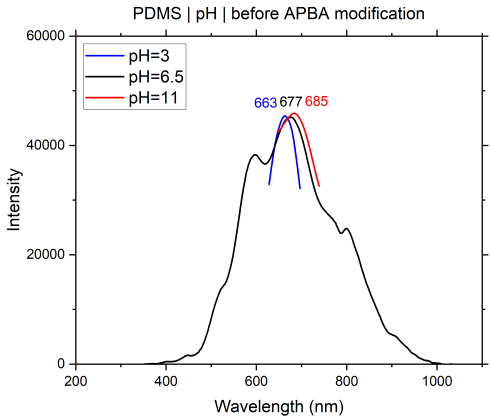

Figure 3.10: Reflectance spectroscopy of an etalon on a PDMS substrate submerged in 1mM HCl/NaCl (pH 3.0), 1mM MQ water/NaCl (pH 6.5) and 1mM NaOH/NaCl (pH 11.0) solutions. 1mM MQ water/NaCl (pH 6.5) is fully shown, for the other two pH levels only the peak wavelength is visualized. The maximum wavelength is also presented for each pH level.

In these pH measurements, it is evident that in more basic environment a red shift of the wavelength occurs. The shift between pH 3.0 to 6.5 is greater than between 6.5 to 11.0. The identical findings were observed when comparing these outcomes with those on a silicon substrate (Fig. 3.5). The reason

could be that the pKa of pNIPAAm is 4.24. Below this threshold, the polymer is neutral and smaller than >4.25, when deprotonation of AAc happens [9, 30, 15]. The shift from pH 3.0 to 6.5 surpasses this treshold. 6.5 and 11.0 are both above the pKa so the effect could be less once the pKa is reached.

3.3.3. Adding plasma treatment to fabrication process

The hydrophobic nature of PDMS presents a significant challenge when creating a monolithic layer of microgel-beads. One potential solution is the utilization of oxygen plasma treatment, where ionized oxygen at high energy can be used to oxidize and create silanol groups (-OH) on the surface of PDMS. This effectively renders the surface more wettable with polar solvents due to the polarity of these silanol groups. Oxygen plasma treatment is favored for treating PDMS surfaces as it offers quick processing time, does not involve chemicals, and provides consistent repeatability in results [34]. Results after plasma treatment are shown in Figure 3.11.

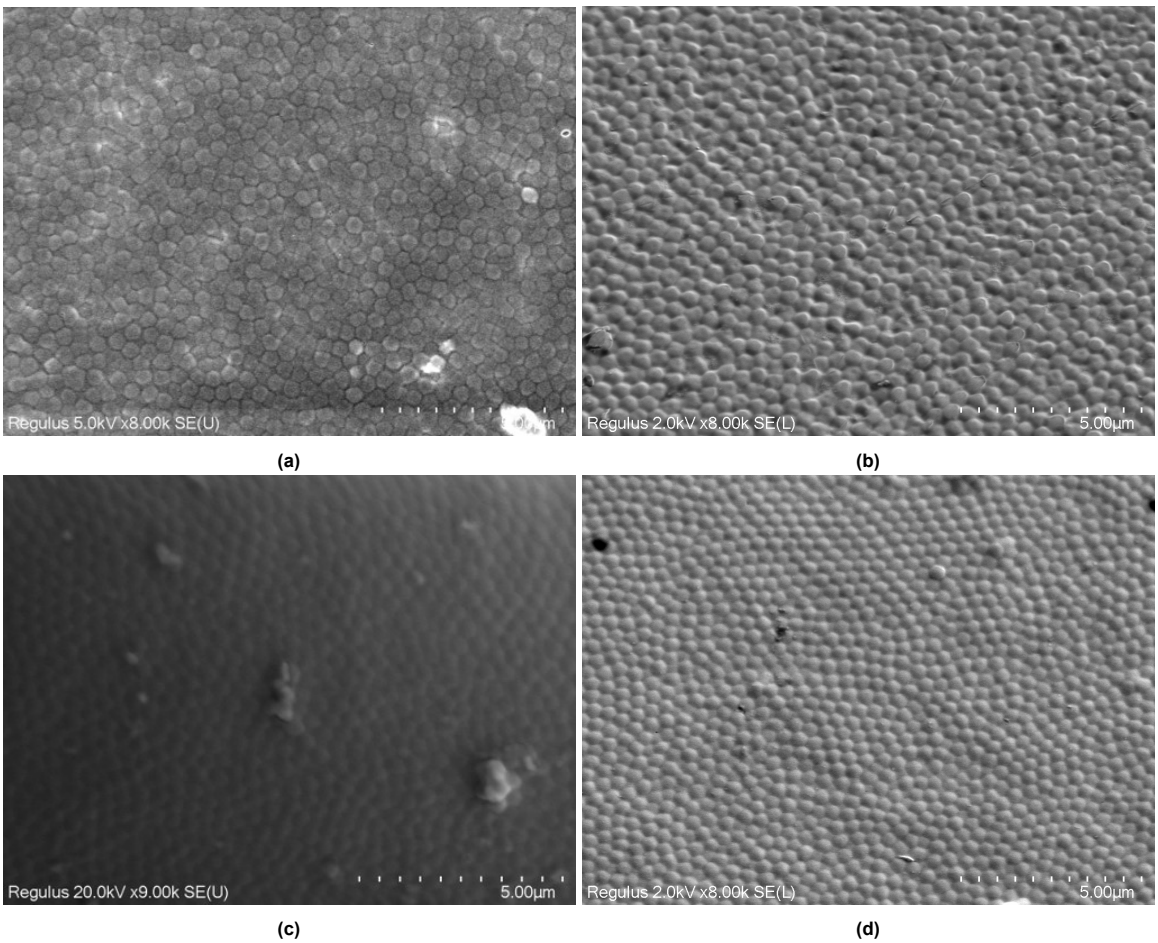

Figure 3.11: SEM images of pNIPAAm-co-10%-AAc mid process **(a)** under 0°angle and **(b)** 30°angle, and post process **(c)** under 0°angle and **(d)** 30°angle. These images were taken after plasma treatment on PDMS substrate.

Plasma treatment prior to spin coating pNIPAAm-co-10%-AAc resulted in the formation of a continuous film. The beads were densely packed without any overlaps or gaps, achieving the desired morphology. However, further validation of the glucose responsiveness was still necessary.

3.3.4. Glucose sensitivity

Reflectance spectroscopy was used to assess the reactivity of the produced etalons to glucose following the same protocol like that of the silicon substrate samples. A calibration curve was made under the same conditions and each samples was measured three times. The mean is shown in Figure 3.12.

Three measurements were conducted per sample. However, three data points from one series of the mid process sample were excluded from the graph due to inconsistencies (further details can be

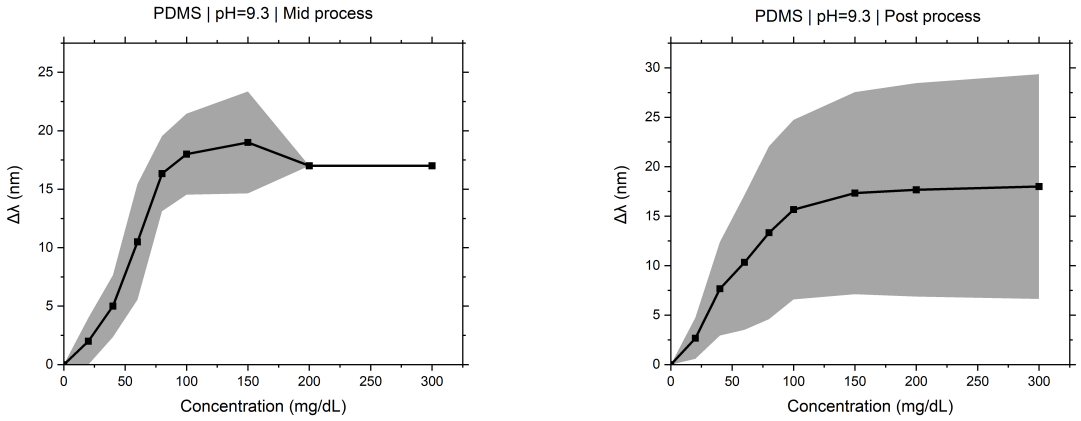

Figure 3.12: Calibration curve of difference in peak wavelength vs. concentration of glucose on PDMS substrate. **(a)** Mid process sample (three measurements with 3 datapoint excluded), and **(b)** post process sample (three measurements). The average of measurements on the same sample are shown, included shaded error bars.

found in Appendix D, Figure D.2). As a result, the calibration curve of the post-process method is considered to be more dependable and uniform. It is anticipated that $\Delta\lambda$ will rise upon contact with a higher concentration of glucose. A comparison of the outcomes from the silicon and PDMS substrates reveals that both show less reliability and consistency in the mid process samples. However, it is evident that the results obtained on the PDMS substrate exhibit greater stability compared to those on the silicon substrate. This variance can be attributed to differences in microbead morphology, with lower density and tighter clustering observed on the PDMS substrate (Fig. 3.12a, b) as opposed to the silicon substrate (Fig. 3.7a, b). These findings validate previous hypotheses regarding how microbead spacing and morphology impacts measurement outcomes.

These experiments demonstrated that PDMS substrates yield similar results to silicon substrates. As a result, further testing on this substrate was decided upon at this stage. Additionally, Bi/ond uses this substrate for their chip, making it sensible to focus on PDMS. Comparison of the mid and post processed samples indicates that post processing provides more reliable results. Consequently, the decision was made to utilize the post processing fabrication technique for subsequent tests involving cell medium and culturing.

3.4. Sterilization process

Sterilization is an important step of the process before organ-on-chip can be in contact with living cells. The same procedure that Bi/ond uses was executed. This contained immersing the etalon in isopropanol and washing it twice in PBS. Other than implementing this step, the same protocol and conditions with the glucose sensitivity measurements were used. The results before and after sterilization are shown in Figure 3.13. Glucose measurements before and after sterilization were performed three and six times, respectively. Also for these series of glucose measurements, $\Delta\lambda$ was monitored as all the series had another λ_{max} baseline (E).

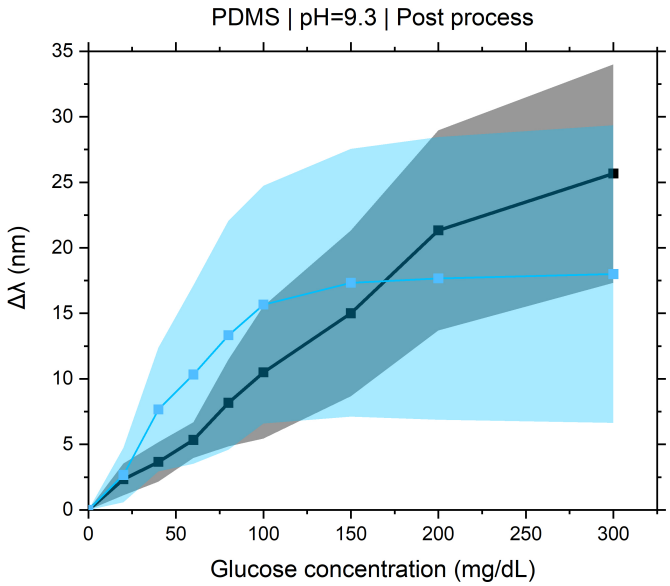

Figure 3.13: Calibration curve of difference in peak wavelength vs. concentration of glucose before (blue, three measurements) and after (black, six measurements) sterilization.

The results in Figure 3.13 demonstrate that the etalons exhibit an improved response to glucose following sterilization. This outcome may be due to the presence of unbound APBA on the post process samples, which could have an adverse effect on the binding of glucose to the responsive microgel-beads. This hypothesis is supported by analyzing of SEM images taken before and after sterilization (Figure 3.14). As discussed previously in section 3.2.1, organic materials bound during the sample processing result in reduced visibility under SEM due to lower conductivity [26]. The comparison between these SEM images shows that the microgel-beads in the sample after sterilization provide a sharper image resolution than those before sterilization. Through this process, all unbound APBA is removed, facilitating the binding of glucose molecules to APBA bound to microgel surface, leading to higher responsivity.

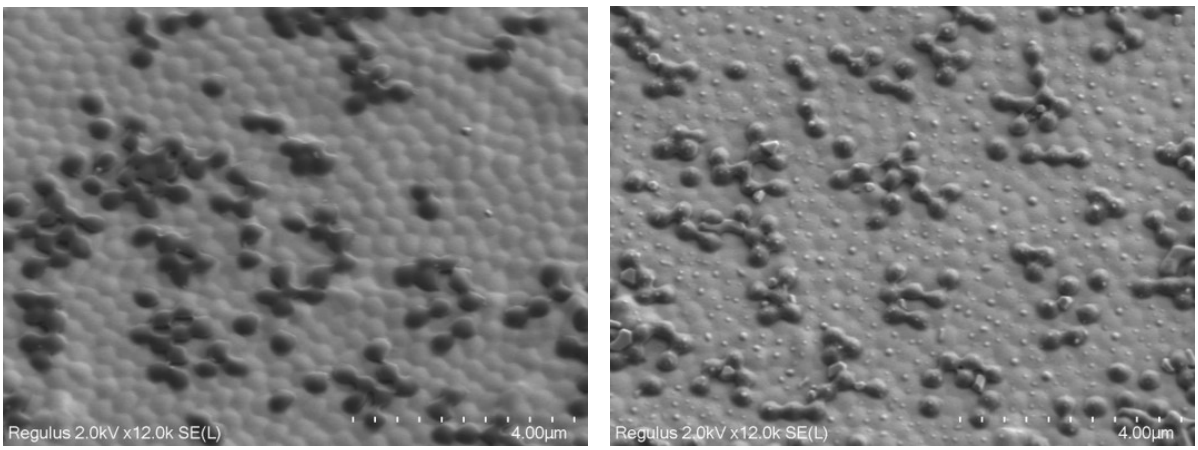

(a) **(b)**

Figure 3.14: SEM images of post process samples **(a)** before and **(b)** after sterilization according to the protocol of Bi/ond.

3.5. Cell medium test

Once it was verified that the etalons continued to function post-sterilization, a cell medium assessment was conducted. This cell medium had been in contact with C_2C_{12} mouse myoblast cells for 1, 3, and 7 days. First, a fresh, sterile, post process PDMS sample was utilized to establish a calibration curve of DMEM medium, which is the same stock medium intended for use in the subsequent cell medium test. A calibration curve for DMEM was created by placing the etalon in the cell medium with glucose concentrations matching those of the glucose calibration line and measuring $\Delta\lambda$. An additional concentration of 450 mg/dL was included to match the original stock medium concentration. This single series of measurements generated the calibration curve. After constructing the calibration curve, the solution in contact with the C_2C_{12} cells was analyzed in triplicate. The outcomes have been adjusted according to the DMEM calibration curve. Figure 3.15 illustrates the findings of both the DMEM calibration curve and the cell medium.

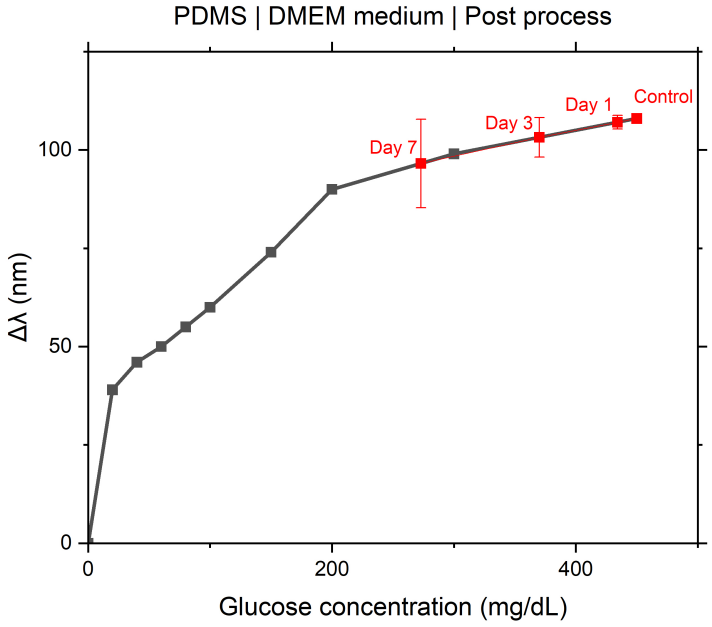

Figure 3.15: Calibration curve of difference in peak wavelength vs. glucose concentration of DMEM medium (measured one time). In red are the results of the decrease in glucose concentration of medium in contact with C_2C_{12} cells for 1, 3, and 7 days (measured three times).

The results show that the concentration of glucose declined approximately 16 mg/dL after day 1, 130 mg/dL after day 3 and 227 mg/dL after day 7, in comparison to the control measurement. The cells utilize glucose as their main energy source, resulting in a decrease in glucose concentration within the medium over time [35]. This can be attributed to APBA forming reversible covalent bonds with cis-1,2 or cis-1,3-diol containing molecules like carbohydrates such as glucose [36]. Before being exposed to C_2C_{12} cells, Bi/ond supplemented the DMEM medium with serum and antibiotics (penicillin and streptomycin) to prevent contamination. This modified DMEM medium served as the control condition and does not contain carbohydrates in the form of serum or antibiotics, thus excluding their influence on the results. DMEM medium primarily includes glucose and no other carbohydrates. It is evident that the reduction in wavelength is solely due to the declining levels of glucose within the medium.

3.6. Cell culture and biocompatibility

The cell medium experiment was an ”indirect” assessment, as the etalon had not yet been exposed to living cells. The next and final step is to conduct cell culturing on the chip and assess biocompatibility. Evaluating biocompatibility is crucial for medical devices that are in contact with tissue. It involves ensuring that a medical device can function as intended without causing any harmful effects [37, 38].

Bi/ond conducted cell culturing of C_2C_{12} mouse myoblast cells based on their custom protocol. The cells were cultured on an etalon, positioned in a 24-well plate, and in a well without etalon (control). The cells were cultured in the wells for two days before microscopic images were captured (Fig. 3.16).

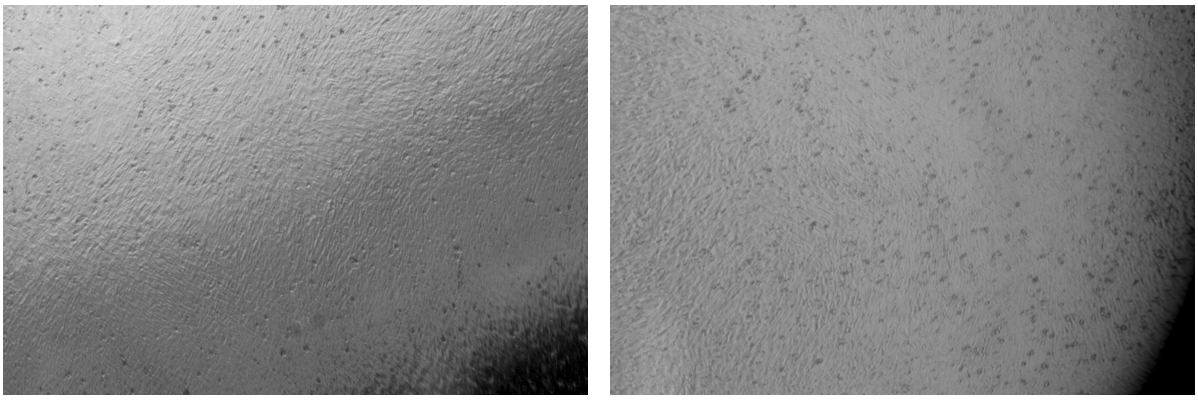

(a) **(b)**

Figure 3.16: Microscopic images taken after two days of culturing C_2C_{12} mouse myoblast cells **(a)** on an etalon on chip and **(b)** in an empty well (control).

The images were taken using an inverted microscope, with the light source positioned below the specimen stage. As a result, only the cells surrounding the chip are captured due to its lack of transparency. However, any potential toxicity from the etalon would affect all cells in the well, not just those on top of the chip. The C_2C_{12} cells exhibited no noticeable difference when cultured on top of or outside the chip, suggesting that etalon material does not impact cell growth and is compatible with culturing. Nonetheless, further biocompatibility tests are necessary for a comprehensive assessment of etalon characteristics.

4

Conclusion

In conclusion, the investigation of this proof-of-concept of glucose responsive microgel-based etalons was successful. This sensor was created on both silicon and PDMS substrate using evaporation of Cr/Au, spin-coating μL pNIPAAm-co-10%-AAc and μL pNIPAAm-co-10%, mid or post process modification with APBA and plasma treatment with oxygen. The fabrication process was optically validated using SEM, while functionality and response were evaluated through reflectance spectroscopy. A calibration curve for glucose was effectively generated for both substrates and modification processes. However, the post process approach proved to be more preferable. The sensor proved resilient to sterilization processes and even exhibited an improved response to glucose due to removal of unbound APBA during sterilization. Post process samples were used to detect changes in glucose levels in cell medium that had been in contact with C_2C_{12} mouse myoblast cells over 1-, 3-, and 7-day periods; indicating decreasing glucose concentrations over time as myoblast cells utilize it as a nutritional source. Additionally, there was optical confirmation of the non-toxic effects of the microgel-beads on cell culturing.

5

Future prospects

An important next step in advancing this proof-of-concept is integrating it into Bi/ond's MUSbit™microfluidic chip. There are several possible placements for this sensor (see Fig. 5.1), each with its advantages and disadvantages. An overview of these pros and cons is provided in Table 5.1.

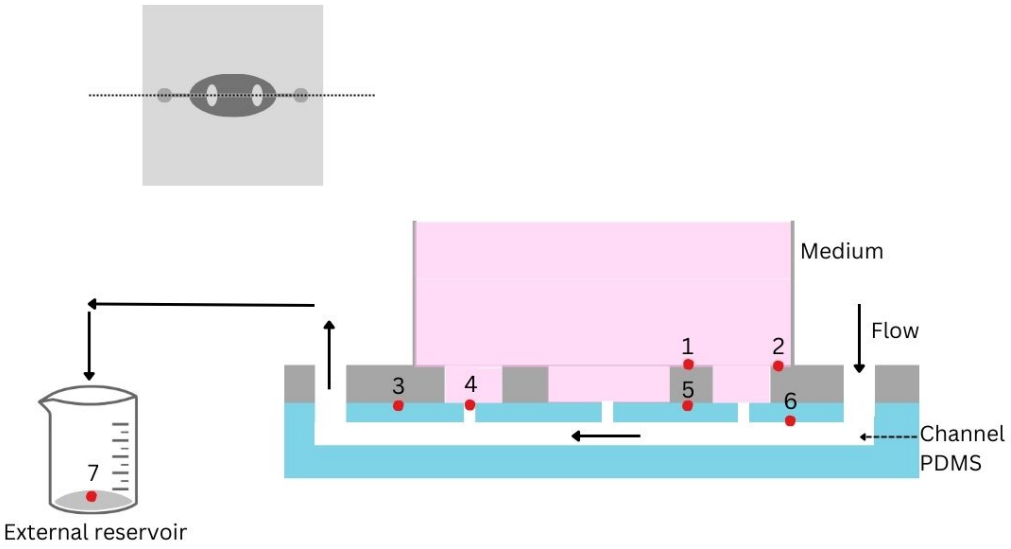

Figure 5.1: Schematic of all the potential placements for the sensor (indicated with red dot+number) in the MUSbit™microfluidic chip of Bi/ond.

The sensor includes Cr and Au, both known as "contaminated" metals in clean room environments. As a result, many pieces of equipment in the clean room cannot be utilized, including those required for fabricating these microfluidic chips. Moreover, during fabrication, hydrogen fluoride (HF) is used - a highly corrosive and toxic substance that should not come into contact with Cr and Au. Hence, sensors 3, 4, 5, and 6 are not recommended to use due to this contamination concern. Another problem that sensor 3 and 5 rise is how they could get in contact with medium. Regarding the other sensors, the majority of information on glucose consumption can be obtained in the well. Therefore, it is not preferable to place it in the channel (sensor 1 and 2 > 6). The flow through the channel is refreshed every 0.45 seconds, which is too rapid for this sensor to detect changes in glucose concentration effectively (sensor 6). Furthermore, if an external reservoir is utilized, the concentration change in flow would be measured rather than in the well (sensor 7). However, this method has an important benefit as it allows the use of the current glucose concentration measurement setup. When the sensor is accessible from the bottom of the chip, glucose changes can be measure from underneath while the cells in the well would still be visible, as an inverted microscope is utilized alongside. However, measuring from above

Table 5.1: Overview of all the advantages and disadvantages of potential placements for sensor in microfluidic chip.

Sensor	Location	Advantage	Disadvantage
1	On top of pillar	Sensor added after fabrication of chip	Vision on cells blocked when measuring
2	On corner of well	Sensor added after fabrication of chip	Vision on cells blocked when measuring
3	Between PDMS layer and well	Measure from bottom $\rightarrow$ Vision on cells	Sensor added during fabrication of chip Not in contact with medium
4	In channel at bottom of well	In contact with medium in well	Sensor added during fabrication of chip
5	Under pillar	Measure from bottom $\rightarrow$ Vision on cells	Sensor added during fabrication of chip Not in contact with medium
6	In channel	Measure from bottom $\rightarrow$ Vision on cells	Sensor added during fabrication of chip Sensor in contact with medium in channel
7	In an external reservoir	Measurement set up same as characterization process	Sensor measures outside of chip and from flow

could pose some challenges as the probe would block vision on the cells from underneath (sensor 1 and 2).
The assessment of all the advantages and disadvantages associated with each position leads to the conclusion that sensor 1 or 2 are most favorable. The main reason being that these can be added after fabrication of the microfluidic chip. Even if this causes visual limitation when executing glucose measurements, cells can be visualized before or after these measurements. A way to overcome this problem is by using a microspectrophotometer. This is a hybrid instrument that merges the magnification capabilities of a light microscope with a UV-visible-NIR (ultraviolet–visible–near infrared) range spectrophotometer[39].

The current way of producing the microgel-based etalons is evaporation and spin-coating. However, with the small dimension of the microfluidic chip of Bi/ond, this may not be the most desired way when upscaling the process. One alternative way of fabricating the sensor could be inkjet printing of microgel-beads. Inkjet printing can be used to print polymers by dissolving the polymer material in a solvent to create an ”ink”. This ink can then be loaded into the inkjet printer. By controlling the deposition of the ink droplets, complex shapes and structures can be printed onto a substrate[40]. This technology could precisely deposit the microgel-beads in the desired place on the microfluidic chip. A subsequent study to examine this possibility could be conducted.

If the sensor is integrated into the microfluidic chip and the preferred fabrication method is determined, the final assessment should involve conducting *in-situ* measurements of glucose in the microfluidic chip. This would allow for utilizing the sensor for its intended function and could provide a solution for non-invasive and continuous real-time analysis of cell viability parameters. If this proves successful, it may lay groundwork for creating other sensors designed to detect substances like lactate.

References

[1] Stefanie Fuchs et al. “In-Line Analysis of Organ-on-Chip Systems with Sensors: Integration, Fabrication, Challenges, and Potential”. In: *ACS Biomaterials Science & Engineering* 7.7 (2021), pp. 2926–2948. DOI: 10.1021/acsbiomaterials.0c01110.

[2] Qasem Ramadan and Mohammed Zourob. “Organ-on-a-chip engineering: Toward bridging the gap between lab and industry”. In: *Biomicrofluidics* 14.4 (2020), p. 041501. DOI: 10.1063/5.0011583.

[3] Johannes Dornhof et al. “Microfluidic organ-on-chip system for multi-analyte monitoring of metabolites in 3D cell cultures”. In: *Lab Chip* 22 (2 2022), pp. 225–239. DOI: 10.1039/D1LC00689D.

[4] Graham A. Clarke et al. “Advancement of Sensor Integrated Organ-on-Chip Devices”. In: *Sensors* 21.4 (2021), p. 1367. DOI: 10.3390/s21041367.

[5] *Musbit - Gobiond*. https://www.gobiond.com/musbit/. Accessed: Monday 11th December, 2023.

[6] Courtney D. Sorrell and Michael J. Serpe. “Glucose sensitive poly (N-isopropylacrylamide) microgel based etalons”. In: *Analytical and Bioanalytical Chemistry* 404.5 (2012), pp. 1234–5678. DOI: 10.1007/s00216-012-5736-x.

[7] Courtney D Sorrell and Michael J Serpe. “Reflection order selectivity of color-tunable poly(N-isopropylacrylamide) microgel based etalons”. In: *Advanced materials (Deerfield Beach, Fla.)* 23.35 (Sept. 2011), pp. 4088–4092. ISSN: 0935-9648. DOI: 10.1002/adma.201101717. URL: https://doi.org/10.1002/adma.201101717.

[8] Yongfeng Gao, Xue Li, and Michael Serpe. “Stimuli-responsive microgel-based etalons for optical sensing”. In: *RSC Adv.* 5 (May 2015). DOI: 10.1039/C5RA02306H.

[9] Andrews Ahiabu and Michael J. Serpe. “Rapidly Responding pH- and Temperature-Responsive Poly(N-Isopropylacrylamide)-Based Microgels and Assemblies”. In: *ACS Omega* 2.5 (2017), pp. 1769–1777. DOI: 10.1021/acsomega.7b00103.

[10] *Etalons Explained*. URL: http://mpo.im/wp-content/uploads/2020/06/TN-2020-06-Etalons-Explained.pdf%5C#:%5C~:text=Etalons%5C%20function%5C%20as%5C%20multiple%5C%20beam%5C%20interferometers%5C%2C%5C%20incident%5C%20light,with%5C%20many%5C%20different%5C%20phases%5C%20through%5C%20the%5C%20whole%5C%20assembly..

[11] Kai C. C. Johnson, Francisco Mendez, and Michael J. Serpe. “Detecting solution pH changes using poly (N-isopropylacrylamide)-co-acrylic acid microgel-based etalon modified quartz crystal microbalances”. In: *Analytica Chimica Acta* 739 (2012), pp. 83–88. DOI: 10.1016/j.aca.2012.06.025.

[12] Zifu Li and To Ngai. “Microgel particles at the fluid–fluid interfaces”. In: *Nanoscale* 5 (4 2013), pp. 1399–1410. DOI: 10.1039/C2NR33503D.

[13] A. Richter et al. “Electronically controllable microvalves based on smart hydrogels: magnitudes and potential applications”. In: *Journal of Microelectromechanical Systems* 12.5 (2003), pp. 748–753. DOI: 10.1109/JMEMS.2003.817898.

[14] Liang Hu and Michael J. Serpe. “Color-Tunable Etalons Assembled from Poly (N-Isopropylacrylamide) Based Microgels”. In: *Polymers* 4.1 (2012), pp. 134–149. DOI: 10.3390/polym4010134.

[15] Molla R Islam et al. “Poly (N-isopropylacrylamide) Microgel-based Optical Devices for Sensing and Biosensing”. In: *Sensors (Basel)* 14.5 (2014), pp. 8984–8995. DOI: 10.3390/s140508984.

[16] Yongfeng Gao, Wenwen Xu, and Michael J. Serpe. “Free-standing poly (N-isopropylacrylamide) microgel-based etalons”. In: *Journal of Materials Chemistry C* 2 (2014), pp. 5878–5884. DOI: 10.1039/C4TC00877D.

[17] Greg Springsteen and Binghe Wang. “A detailed examination of boronic acid–diol complexation”. In: *Tetrahedron* 58.26 (2002), pp. 5291–5300. ISSN: 0040-4020. DOI: https://doi.org/10.1016/S0040-4020(02)00489-1. URL: https://www.sciencedirect.com/science/article/pii/S0040402002004891.

[18] “Chapter Five - Proximal Soil Sensing: An Effective Approach for Soil Measurements in Space and Time”. In: *Advances in Agronomy*. Ed. by Donald L. Sparks. Vol. 113. Advances in Agronomy. Academic Press, 2011, pp. 243–291. DOI: https://doi.org/10.1016/B978-0-12-386473-4.00005-1. URL: https://www.sciencedirect.com/science/article/pii/B9780123864734000051.

[19] Bruce Hapke. “Reflectance Methods and Applications”. In: *Encyclopedia of Spectroscopy and Spectrometry (Third Edition)*. Ed. by John C. Lindon, George E. Tranter, and David W. Koppenaal. Third Edition. Oxford: Academic Press, 2017, pp. 931–935. ISBN: 978-0-12-803224-4. DOI: https://doi.org/10.1016/B978-0-12-803224-4.00019-4. URL: https://www.sciencedirect.com/science/article/pii/B9780128032244000194.

[20] “PDMS with designer functionalities—Properties, modifications strategies, and applications”. In: *Progress in Polymer Science* 83 (2018), pp. 97–134. ISSN: 0079-6700. DOI: https://doi.org/10.1016/j.progpolymsci.2018.06.001. URL: https://www.sciencedirect.com/science/article/pii/S0079670017300783.

[21] J.M. Anderson. “9.19 - Biocompatibility”. In: *Polymer Science: A Comprehensive Reference*. Ed. by Krzysztof Matyjaszewski and Martin Möller. Amsterdam: Elsevier, 2012, pp. 363–383. ISBN: 978-0-08-087862-1. DOI: https://doi.org/10.1016/B978-0-444-53349-4.00229-6. URL: https://www.sciencedirect.com/science/article/pii/B9780444533494002296.

[22] Buddy D. Ratner and Frederick J. Schoen. “2.3.2 - The Concept and Assessment of Biocompatibility”. In: *Biomaterials Science (Fourth Edition)*. Ed. by William R. Wagner et al. Fourth Edition. Academic Press, 2020, pp. 843–849. ISBN: 978-0-12-816137-1. DOI: https://doi.org/10.1016/B978-0-12-816137-1.00056-8. URL: https://www.sciencedirect.com/science/article/pii/B9780128161371000568.

[23] Courtney D. Sorrell, Matthew C. D. Carter, and Michael J. Serpe. “A ”paint-on” protocol for the facile assembly of uniform microgel coatings for color tunable etalon fabrication.” In: *ACS applied materials & interfaces* 3 4 (2011), pp. 1140–7. URL: https://api.semanticscholar.org/CorpusID:21149588.

[24] Elizaveta Burdukova et al. “Temperature controlled surface hydrophobicity and interaction forces induced by poly (N-isopropylacrylamide)”. In: *Journal of colloid and interface science* 342.2 (2010), pp. 586–592. ISSN: 1095-7103. DOI: 10.1016/j.jcis.2009.10.049. URL: https://doi.org/10.1016/j.jcis.2009.10.049.

[25] Taolei Sun et al. “Reversible Switching between Superhydrophilicity and Superhydrophobicity”. In: *Angewandte Chemie International Edition* 43.3 (2004), pp. 357–360. DOI: https://doi.org/10.1002/anie.200352565. URL: https://onlinelibrary.wiley.com/doi/abs/10.1002/anie.200352565.

[26] Longjian Xue, Jilin Zhang, and Yanchun Han. “Phase separation induced ordered patterns in thin polymer blend films”. In: *Progress in Polymer Science* 37.4 (2012). Topical Issue on Polymer Physics, pp. 564–594. ISSN: 0079-6700. DOI: https://doi.org/10.1016/j.progpolymsci.2011.09.001. URL: https://www.sciencedirect.com/science/article/pii/S0079670011001067.

[27] Hollis Williams. “SEM for conductive and non-conductive specimens”. In: *Physics Education* 56.5 (Aug. 2021), p. 055034. DOI: 10.1088/1361-6552/ac1503. URL: https://dx.doi.org/10.1088/1361-6552/ac1503.

[28] Shuaipeng Wang et al. “Taking advantages of intramolecular hydrogen bonding to prepare mechanically robust and catalyst-free vitrimer”. In: *Polymer* 210 (2020), p. 123004. ISSN: 0032-3861. DOI: https://doi.org/10.1016/j.polymer.2020.123004. URL: https://www.sciencedirect.com/science/article/pii/S0032386120308296.

[29] Samuel J Ling, Jeff Sanny, and William Moebs. *University Physics*. Sept. 2016.

[30] Matthias Karg et al. “Nanogels and Microgels: From Model Colloids to Applications, Recent Developments, and Future Trends”. In: *Langmuir* 35.19 (2019), pp. 6231–6255. DOI: 10.1021/acs.langmuir.8b04304.

[31] Abraham Belkind and Sophia Gershman. “Plasma cleaning of surfaces”. In: *Vac. Technol. Coat.* (Jan. 2008), pp. 1–11.

[32] Svetoslav V. Nikolov, Alberto Fernandez-Nieves, and Alexander Alexeev. “Behavior and mechanics of dense microgel suspensions”. In: *Proceedings of the National Academy of Sciences* 117.44 (2020), pp. 27096–27103. DOI: 10.1073/pnas.2008076117. URL: https://www.pnas.org/doi/abs/10.1073/pnas.2008076117.

[33] Sarah-Sophia D. Carter et al. “PDMS leaching and its implications for on-chip studies focusing on bone regeneration applications”. In: *Organs-on-a-Chip* 2 (2020), p. 100004. ISSN: 2666-1020. DOI: https://doi.org/10.1016/j.ooc.2020.100004. URL: https://www.sciencedirect.com/science/article/pii/S2666102020300045.

[34] Bruce K. Gale et al. “Low-Cost MEMS Technologies”. In: *Comprehensive Microsystems*. Ed. by Yogesh B. Gianchandani, Osamu Tabata, and Hans Zappe. Oxford: Elsevier, 2008, pp. 341–378. ISBN: 978-0-444-52190-3. DOI: https://doi.org/10.1016/B978-044452190-3.00011-2. URL: https://www.sciencedirect.com/science/article/pii/B9780444521903000112.

[35] Tugba Kilic et al. “Organs-on-chip monitoring: sensors and other strategies”. In: *Microphysiological Systems* 2.0 (2018). DOI: 10.21037/MPS.2018.01.01.

[36] Xixi Sun et al. “Catalyst recognition of cis-1,2-diols enables site-selective functionalization of complex molecules”. In: *Nature chemistry* 5.9 (2013), pp. 790–795. ISSN: 1755-4349. DOI: 10.1038/nchem.1726. URL: https://doi.org/10.1038/nchem.1726.

[37] Martin Augustynek et al. “Biocompatibility of Medical Devices and Their Risks”. In: Oct. 2019, pp. 228–231. DOI: 10.1109/EUVIP47703.2019.8946251.

[38] Yimin Qin. “Qin2016”. In: *Medical Textile Materials*. Ed. by Yimin Qin. Woodhead Publishing Series in Textiles. Woodhead Publishing, 2016, pp. 191–201. ISBN: 978-0-08-100618-4. DOI: https://doi.org/10.1016/B978-0-08-100618-4.00014-5. URL: https://www.sciencedirect.com/science/article/pii/B9780081006184000145.

[39] Paul Martin. “Spectroscopy with a Light Optical Microscope”. In: *Microscopy Today* 21.1 (2013), pp. 22–26. DOI: 10.1017/S1551929512001034.

[40] de Bj Berend-Jan Gans, P. C. Duineveld, and US Ulrich Schubert. *Inkjet Printing of Polymers: State of the Art and Future Developments*. Feb. 2004. DOI: https://doi.org/10.1002/adma.200300385. URL: https://doi.org/10.1002/adma.200300385.

A

Pattern etalons

The initial attempt to produce an etalon involved covering a 525 μm n-type silicon wafer with aluminum foil and manually creating holes in it. These holes varied in size, with the largest being 8 mm (Fig. A.1(b)). The outcomes after depositing the first layer of Cr/Au are displayed in Fig. A.1(b).

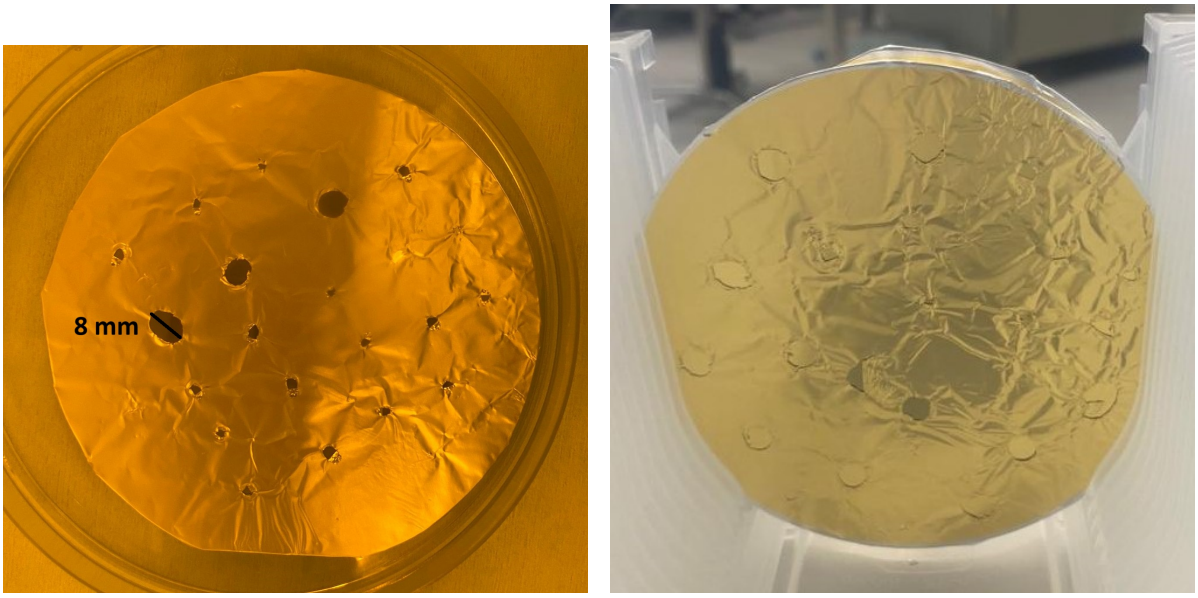

(a) (b)

Figure A.1: First attempt trying to make an etalon with (a) a silicon wafer wrapped in aluminium foil and (b) the result after evaporating the first Cr/Au layer.

After applying pNIPAAm-co-10%-AAc to approximately half of the Cr/Au areas using spin-coating, the substrate's appearance resembled that in Fig. A.2(a). The smudges visible on the surface indicate where pNIPAAm-co-10%-AAc was pipetted and spin-coated. Subsequently, the wafer was placed in a 30°C furnace overnight, following which the second layer of Cr/Au was evaporated. Only the intended areas remained exposed; the rest was covered with tape (A.2(b)).

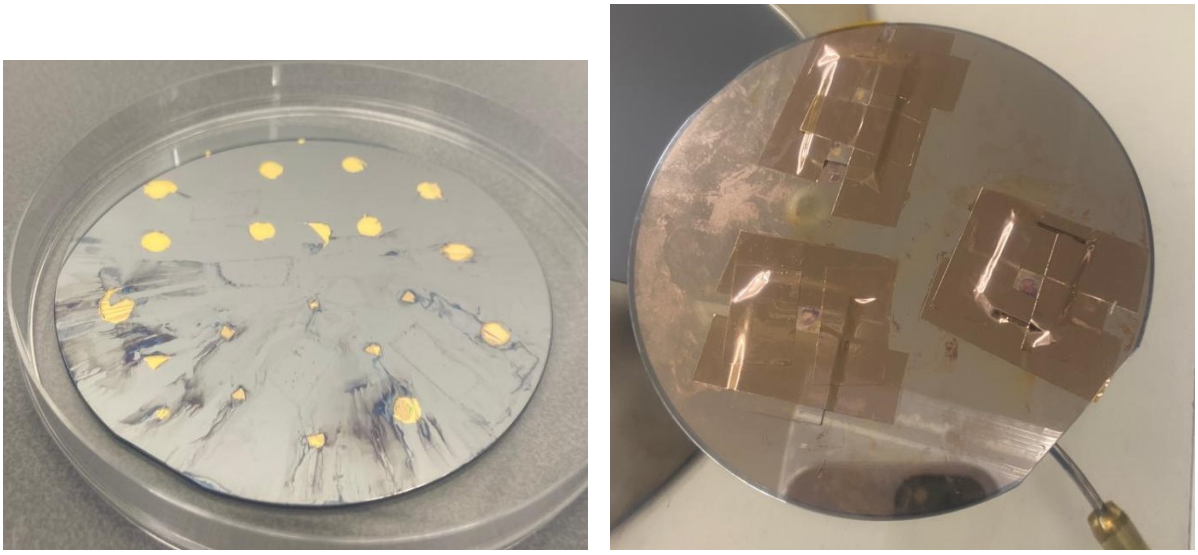

(a) (b)

Figure A.2: The look of the silicon wafer (a) after spin-coating pNIPAAm-co-10%-AAc on half of the Cr/Au areas and (b) after desposition of the second layer of Cr/Au.

To create a consistent pattern for the etalons, stainless steel sheets with a thickness of 0.1 mm (1.4310) and dimensions of 20 by 20 mm were produced, containing holes ranging from 0.5-3 mm in diameter. The design schematic can be found in Section 2.2. Figure A.3 displays an image of the samples attached to a wafer after the first layer of Cr/Au was evaporated using the sheet masks.

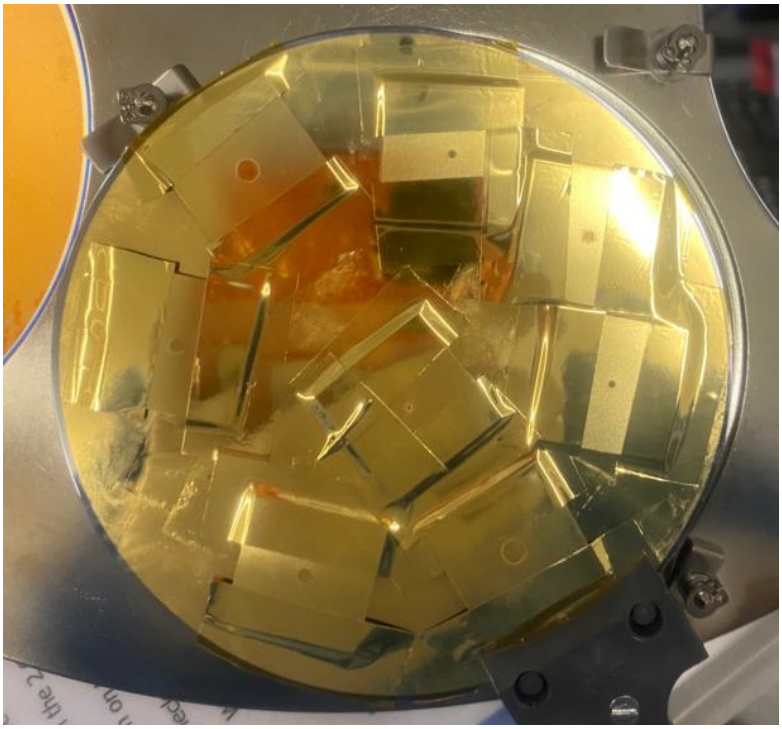

Figure A.3: Picture of samples taped onto a wafer after evaporating the first layer of Cr/Au with the sheet masks

B

Samples

Table B.1: Overview of samples made during this thesis.

Version	Substrate	Polymer Spincoating	Velocity (rmp)	Ramp (rpm/s)	Volume (µL)	Mask material	n	Size (mm)	Functionalization
1	Si	pNIPAm-co-10%AAC	2000	1000	5	Aluminium	1	~3	Post Process
1	Si	pNIPAm-co-10%AAC	3000	2000	5	Aluminium	1	~3	Post Process
1	Si	pNIPAm-co-10%AAC-APBA	2000	1000	5	Aluminium	1		Synthesis
1	Si	pNIPAm-co-10%AAC-APBA	3000	2000	5	Aluminium	1		Synthesis
2	Si	pNIPAm-co-10%AAC	3000	2000	5	Stainless steel	1	3	Post Process
2	Si	pNIPAm-co-10%AAC	3000	2000	5	Stainless steel	1	2	Mid Process
2	Si	pNIPAm-co-10%AAC	3000	2000	3	Stainless steel	1	1	Post Process
2	Si	pNIPAm-co-10%AAC	3000	2000	3	Stainless steel	1	0.5	Post Process
2	Si	pNIPAm-co-10%AAC-APBA	3000	2000	5	Stainless steel	1	3	Synthesis
2	Si	pNIPAm-co-10%AAC-APBA	3000	2000	5	Stainless steel	1	2	Synthesis
2	Si	pNIPAm-co-10%AAC-APBA	3000	2000	3	Stainless steel	1	1	Synthesis
2	Si	pNIPAm-co-10%AAC-APBA	3000	2000	3	Stainless steel	1	0.5	Synthesis
2	Si+PDMS	pNIPAm-co-10%AAC	3000	2000	5	Stainless steel	1	3	Post Process
2	Si+PDMS	pNIPAm-co-10%AAC	3000	2000	5	Stainless steel	1	2	Mid Process
2	Si+PDMS	pNIPAm-co-10%AAC	3000	2000	3	Stainless steel	1	1	Post Process
2	Si+PDMS	pNIPAm-co-10%AAC	3000	2000	3	Stainless steel	1	0.5	Post Process
2	Si+PDMS	pNIPAm-co-10%AAC-APBA	3000	2000	5	Stainless steel	1	3	Synthesis
2	Si+PDMS	pNIPAm-co-10%AAC-APBA	3000	2000	5	Stainless steel	1	2	Synthesis
2	Si+PDMS	pNIPAm-co-10%AAC-APBA	3000	2000	3	Stainless steel	1	1	Synthesis
2	Si+PDMS	pNIPAm-co-10%AAC-APBA	3000	2000	3	Stainless steel	1	0.5	Synthesis
2.5	Si+PDMS	pNIPAm-co-10%AAC	1000	1000	5	Stainless steel	4	1	Post Process
2.5	Si+PDMS	pNIPAm-co-10%AAC	1000	1000	5	Stainless steel	3	3	Post Process
2.5	Si+PDMS	pNIPAm-co-10%AAC-APBA	1000	1000	5	Stainless steel	1	3	Synthesis

Table B.2: Overview of samples made during this thesis.

Version	Substrate	Polymer Spincoating	Velocity (rmp)	Ramp (rpm/s)	Volume (µL)	Mask material	n	Size (mm)	Functionalization
3	Si	pNIPAm-co-10%AAC	3000	2000	5	Stainless steel	1	3	Mid Process
3	Si	pNIPAm-co-10%AAC	3000	2000	5	Stainless steel	1	3	Post Process
3	Si	pNIPAm-co-10%AAC	3000	2000	5	Stainless steel	1	3	Post Process
3	Si+PDMS	pNIPAm-co-10%AAC	3000	2000	5	Stainless steel	1	3	Mid Process
3	Si+PDMS	pNIPAm-co-10%AAC	3000	2000	5	Stainless steel	1	3	Post Process
3	Si+PDMS	pNIPAm-co-10%AAC	3000	2000	5	Stainless steel	1	3	Post Process
4	Si	pNIPAm-co-10%AAC	3000	2000	5	Stainless steel	5	3	Mid Process
4	Si+PDMS	pNIPAm-co-10%AAC	3000	2000	5	Stainless steel	5	3	Mid Process
5	Si	pNIPAm-co-10%AAC	3000	2000	5	Stainless steel	1	3	Mid Process
5	Si	pNIPAm-co-10%AAC	3000	2000	5	Stainless steel	1	3	Post-Proces
5	Si+PDMS	pNIPAm-co-10%AAC	3000	2000	5	Stainless steel	1	3	Mid Process
5	Si+PDMS	pNIPAm-co-10%AAC	3000	2000	5	Stainless steel	1	3	Post-Proces
6	Si	pNIPAm-co-10%AAC	3000	2000	5	Stainless steel	2	3	Mid Process
6	Si	pNIPAm-co-10%AAC	3000	2000	5	Stainless steel	2	3	Post-Proces
6	Si+PDMS	pNIPAm-co-10%AAC	3000	2000	5	Stainless steel	2	3	Mid Process
6	Si+PDMS	pNIPAm-co-10%AAC	3000	2000	5	Stainless steel	2	3	Post-Proces
7	Si+PDMS	pNIPAm-co-10%AAC	3000	2000	5	Stainless steel	5	3	Mid Process
7	Si+PDMS	pNIPAm-co-10%AAC	3000	2000	5	Stainless steel	5	3	Post-Proces

C

Samples silicon substrate

To confirm its responsiveness to temperature, the initial samples produced with an aluminum mask were tested. The samples were exposed to 1mM MQ water/NaCl (pH 6.5) at temperatures of 22°C and 35°C. The results are presented in Figure C.1.

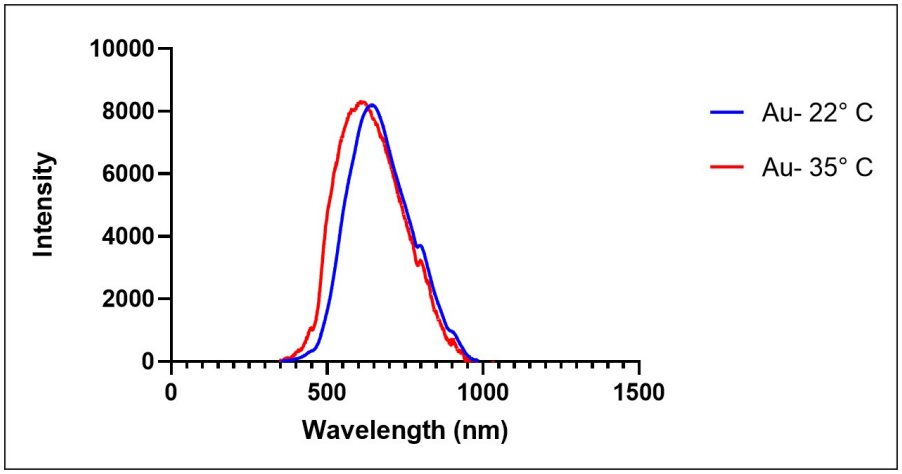

Figure C.1: Results of first test to validate functionalization of etalons with temperature using an aluminium mask. pH 6.5

Functionalization of the etalons with APBA was confirmed by subjecting them to a glucose environment, resulting in a peak shift with an increase in temperature. The initial step involved creating a glucose dilution line by dissolving glucose in MiliQ water with a pH level of 6.5. The outcomes of this initial experiment are illustrated in Fig. C.2.

A shift in the peak was observed as the temperature increased. The next stage involved confirming the etalons' functionalization with APBA by exposing them to a glucose environment. A dilution line of glucose was initially created by dissolving it in MiliQ water, resulting in a pH level of 6.5. The findings from this initial attempt are visualized in Fig. C.2.

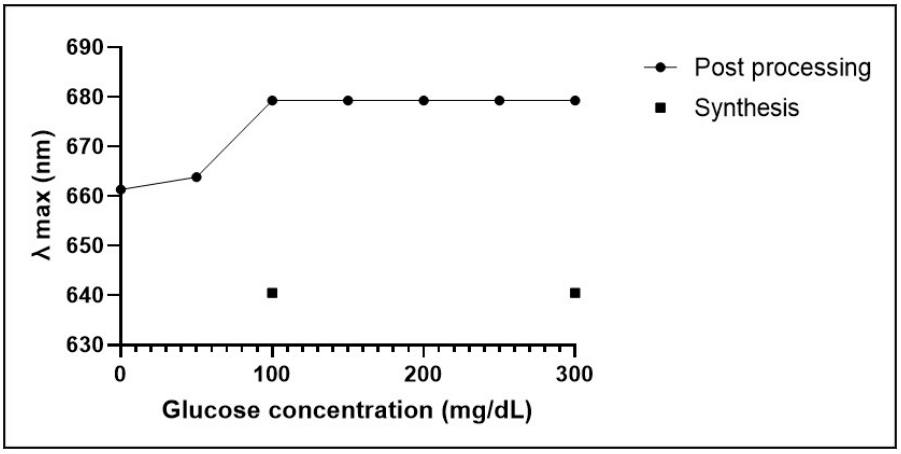

Figure C.2: Results of first test to validate functionalization of etalons with glucose using an aluminium mask. pH 6.5

A platform was achieved, and there were no changes in the peaks for the synthesized sample. Because this outcome seemed unlikely, modifications were implemented to the measurement approach: more concentrations were included in the lower range, and extra attention was given to thoroughly clean the tip of the reflectance spectrometer probe between each measurement. With these adjustments, a new calibration curve was generated. Figure C.3 displays the results obtained.

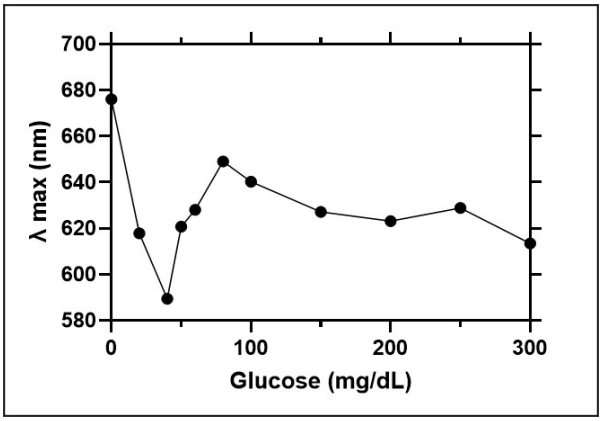

Figure C.3: Attempt to create a new calibration curve with additional concentrations in lower region and properly cleaning of tip of probe (mid process sample). pH 6.5

The reliability of the results was questionable due to significant fluctuations in the maximum wavelength. To address this, a new calibration curve was constructed using pre-made glucose concentrations diluted in 5mM Na_2CO_3/$NaHCO_3$ buffer (pH 9.3), as it is considered most suitable for the microgel-beads ([6]). Additionally, a modification was made to the process for measuring λ_{max}, with the whole sample fully immersed in liquid instead of adding a drop between the probe's end and the sample. The outcomes are illustrated in C.4.

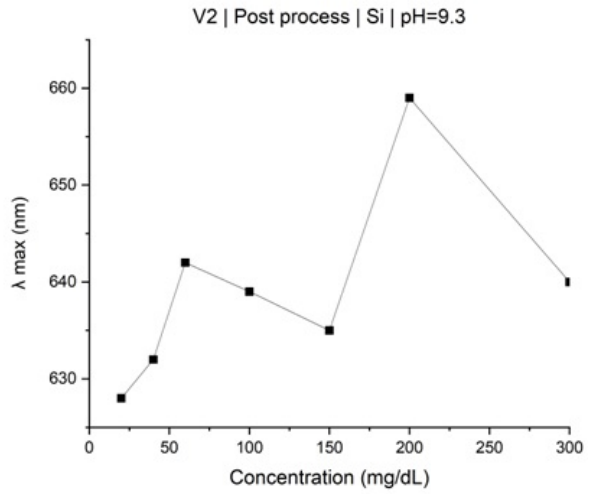

Figure C.4: Results of post process samples after submerging the whole sample in liquid.

After conducting numerous measurements to familiarize oneself with the measurement technique and ensure consistent execution of each step, improvements in the outcomes were observed, particularly for the post processing sample. Conversely, the mid processing sample appeared to exhibit the opposite effect (Fig. C.5).

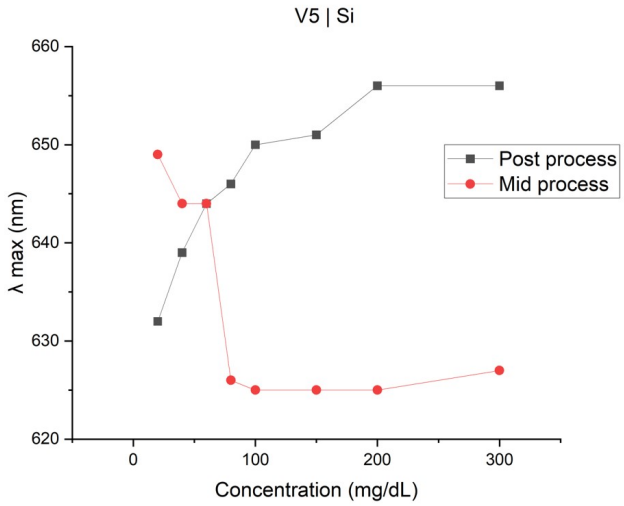

Figure C.5: Calibration curve after multiple attempt to create calibration curve on mid and post process samples. pH 9.3

Efforts were made to replicate the post process curve and enhance the accuracy of measurements on mid process samples. One sample was used three times to a calibration curve. Since the baseline of each measurement was different, also $\Delta\lambda$ was plotted. The findings for mid process samples are shown in Fig. C.6, while those for post processing are illustrated in Fig. C.7.

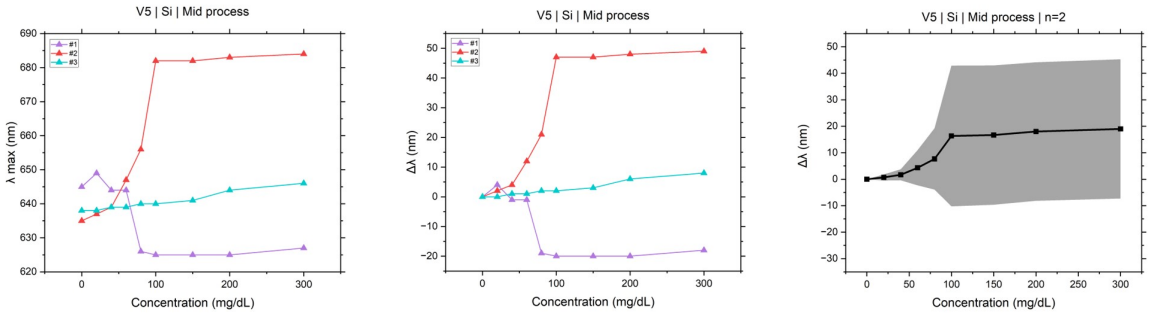

(a) **(b)** **(c)**

Figure C.6: Reflectance spectroscopy graphs of calibration curve on mid process sample. One sample was measured three times. (a) shows the λ_{max}-glucose concentration plot, (b) $\Delta\lambda$-glucose concentration plot, measurement serie 3 (purple) was not included in (c) the average value of $\Delta\lambda$-glucose concentration plot with shaded error bars. (pH 9.3)

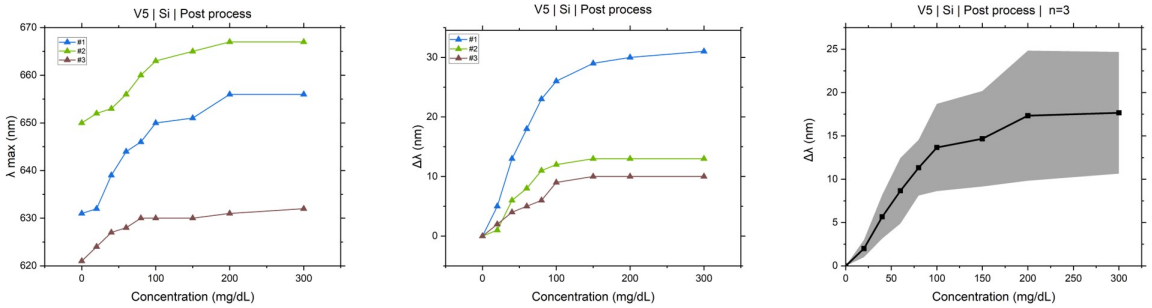

(a) **(b)** **(c)**

Figure C.7: Reflectance spectroscopy graphs of calibration curve on post process sample. One sample was measured three times. (a) shows the λ_{max}-glucose concentration plot, (b) $\Delta\lambda$-glucose concentration plot, (c) the average value of $\Delta\lambda$-glucose concentration plot with shaded error bars. (pH 9.3)

The results on the post process sample looked more reliable than the mid processed one. The measurement serie where the mid processing sample appeared to exhibit the opposite effect was not included in the average $\Delta\lambda$-glucose concentration plot.

Based on these resultsThe omission of certain concentrations resulted in a discernible pattern in the calibration curve. Following these results, it was determined that the post processing method of chemical modification with APBA was preferable, and due to PDMS being the utilized substrate by Bi/ond, it was decided to further conduct cell testing using this substrate.

D

Samples PDMS substrate

All experiments conducted on the silicon substrate were also simultaneously carried out on the PDMS substrate. For this substrate, only pH 9.3 was used because when we started using this material, we already figured out that this was most suitable for the microgel-beads[6]. The initial attempt to produce a glucose calibration curve on a mid process sample yielded unreliable outcomes (Fig. D.1). However, when certain concentrations were excluded, a pattern in the calibration curve became noticeable.

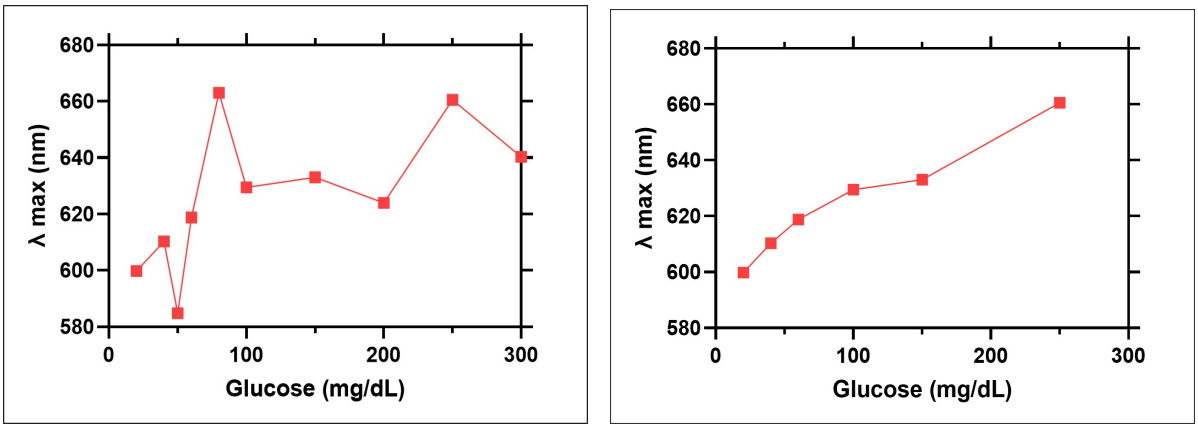

Figure D.1: Reflectance spectroscopy graphs of **(a)** first attempt to create glucose calibration curve on mid process sample. When excluding some of the data points **(b)** a pattern in the calibration curve became noticeable.

This pattern was tried to recreate and after a lot of repeatedly testing, the results started to look promising. Therefore, similar like on silicon substrate, one sample was tested three times and a calibration curve was created by taking the average of these three measurements. The results of the mid process sample are displayed in Figure D.2, while the post process results are shown in Figure D.3.

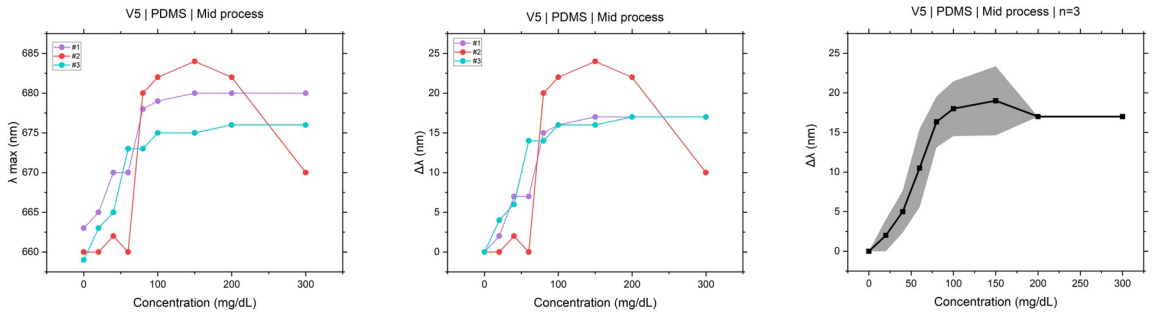

(a) **(b)** **(c)**

Figure D.2: Reflectance spectroscopy graphs of calibration curve on mid process sample. One sample was measured three times. (a) shows the λ_{max}-glucose concentration plot, (b) $\Delta\lambda$-glucose concentration plot, the 4th and last concentration of serie 2 (red) was not included in (c) the average value of $\Delta\lambda$-glucose concentration plot with shaded error bars. (pH 9.3)

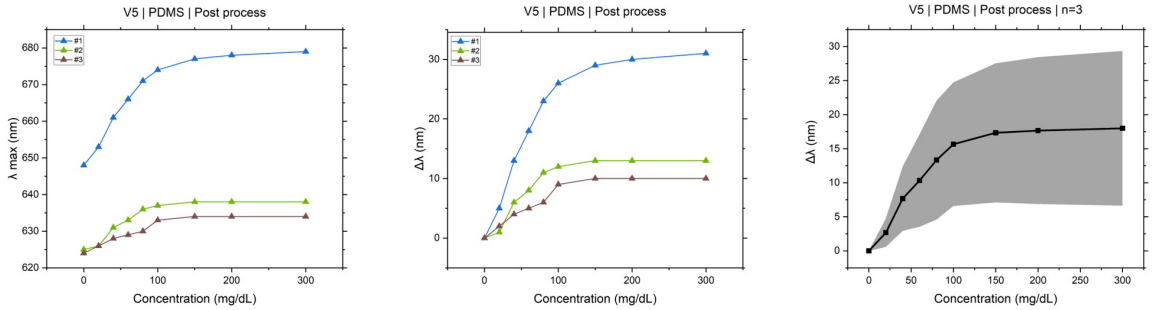

(a) **(b)** **(c)**

Figure D.3: Reflectance spectroscopy graphs of calibration curve on post process sample. One sample was measured three times. (a) shows the λ_{max}-glucose concentration plot, (b) $\Delta\lambda$-glucose concentration plot, (c) the average value of $\Delta\lambda$-glucose concentration plot with shaded error bars. (pH 9.3)

The findings suggest that the post processed samples yielded more dependable results, indicating that this method is preferable for conducting further cell tests.

E

Sterilization

Individual results of glucose measurements on mid (Figure E.1) and post (Figure E.2) process samples.

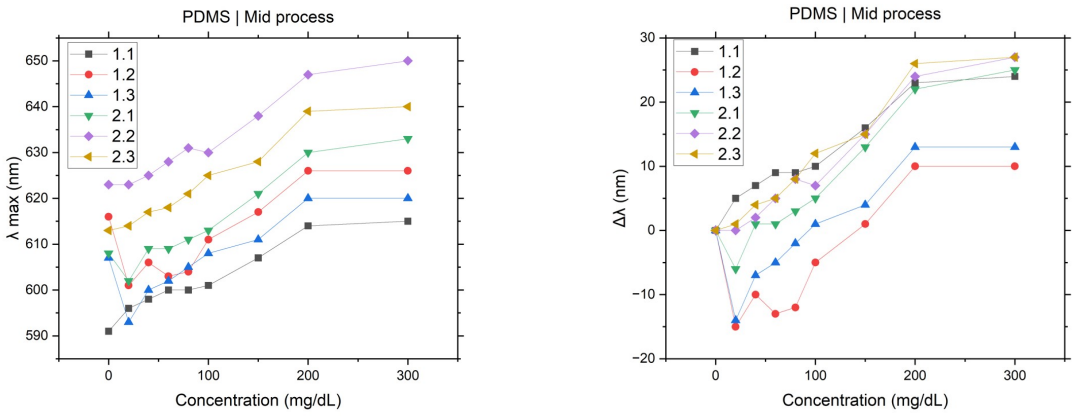

(a) **(b)**

Figure E.1: Individual measurements on mid process samples after sterilization. The λ_{max} baseline for every measurement serie was different, therefore, $\Delta\lambda$ was monitored as well. Two samples were each measured 3 times, resulting in a total of six measurement after sterilization.

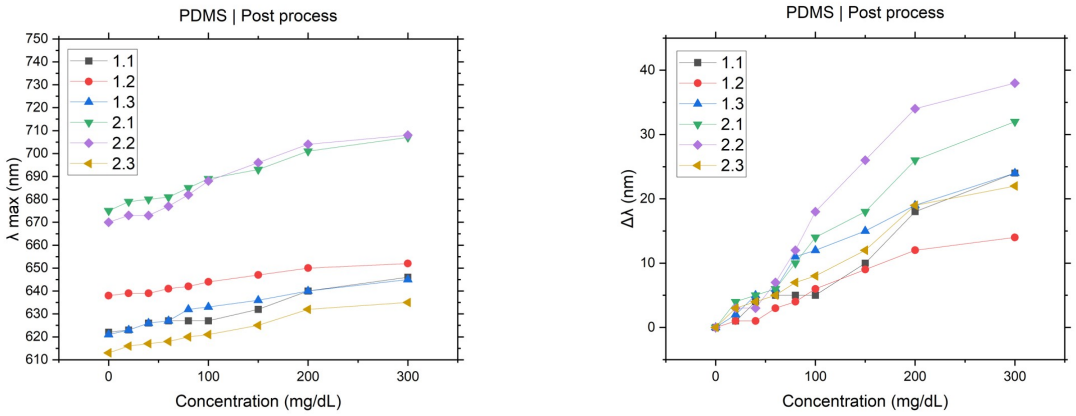

Figure E.2: Individual measurements on post process samples after sterilization. The λ_{max} baseline for every measurement serie was different, therefore, $\Delta\lambda$ was monitored as well. Two samples were each measured 3 times, resulting in a total of six measurement after sterilization.